1 **Hypertrophic adipocytes increase extracellular vesicle-mediated lipid release and reprogram breast**
2 **cancer cell metabolism**

3 Garrett F Beeghly[1], Marlee I Pincus[1], Rohan R Varshney[2], Dilip D Giri[3], Domenick J Falcone[4], Michael C
4 Rudolph[2], Marc A Antonyak[5], Neil M Iyengar[6,7], and Claudia Fischbach[1,8]

5
6 1. Nancy E. and Peter C. Meinig School of Biomedical Engineering, Cornell University, Ithaca, NY, USA
7 2. Harold Hamm Diabetes Center and Department of Physiology, University of Oklahoma Health Sciences
8   Center, Oklahoma City, OK, USA
9 3. Department of Pathology, Memorial Sloan Kettering Cancer Center, New York, NY, USA
10 4. Department of Pathology and Laboratory Medicine, Weill Cornell Medical College, New York, NY, USA
11 5. Department of Molecular Medicine, Cornell University, Ithaca, NY, USA
12 6. Department of Medicine, Memorial Sloan Kettering Cancer Center, New York, NY, USA
13 7. Department of Medicine, Weill Cornell Medical College, New York, NY, USA
14 8. Kavli Institute at Cornell for Nanoscale Science, Cornell University, Ithaca, NY, USA

15
16 Correspondence to cf99@cornell.edu

17

18 **Abstract**

19 Obesity worsens cancer-specific survival and all-cause mortality for women diagnosed with breast cancer.
20 Rich in adipose tissue, the breast exhibits increased adipocyte size in obesity, which correlates with poor
21 prognosis. However, adipocyte size is highly heterogeneous as adipose tissue expands through both
22 hyperplasia and hypertrophy; and adipocyte size can increase independently of weight gain. Despite these
23 observations, the impact of adipocyte size on breast cancer cell behavior remains unclear due to insufficient
24 approaches to isolate adipocytes based on size and maintain them in culture for mechanistic studies. Here,
25 we develop strategies to culture size-sorted adipocytes from two mouse models of obesity and test their
26 functional impact on tumor cell malignancy. We find that large adipocytes are transcriptionally distinct from
27 small adipocytes and are enriched for gene sets related to adipose tissue dysfunction, including altered lipid
28 processing. In coculture studies, large adipocytes promote lipid accumulation in breast cancer cells, and
29 enhance their migration, proliferation, and aerobic metabolism in a manner dependent on fatty acid oxidation.
30 These changes coincide with increased release of extracellular vesicles by large versus small adipocytes,
31 which transfer lipid to recipient tumor cells. Moving forward, our findings suggest that adipocyte size could
32 serve as a prognostic biomarker for women with breast cancer and help identify new therapeutic targets to
33 advance clinical outcomes for these patients.

34

35 **Introduction**
36 Over 40% of adult women in the U.S. are obese[1] and obesity is an established prognostic factor associated
37 with poor clinical outcomes across all breast cancer subtypes[2]. Obesity is a complex disease with multivariate
38 pathophysiology, including endocrine dysfunction, altered metabolism, and systemic inflammation[3]. As a
39 result, previous research has focused on how obesity-mediated changes to hormone signaling[4], lipid
40 homeostasis[5], and anti-tumor immunity[6] impact carcinogenesis. However, given the critical role of contextual
41 cues in tumor progression, obesity-mediated changes to the local microenvironment are also an important
42 consideration. For breast cancer, this includes remodeling of white adipose tissue (WAT) which forms a
43 primary component of the mammary stroma. Nevertheless, our mechanistic understanding of how obesity
44 impacts breast cancer prognosis through changes at both the tissue and organism level remains limited.

45

46 Recent studies indicate that adipocytes, which are the functional units of WAT, are more plastic[7,8] and
47 heterogenous[9,10] than once considered and comprise distinct subpopulations which change in obesity.
48 Enlarged or hypertrophic adipocytes are one subpopulation of interest, as increased mammary adipocyte
49 size correlates with the transition from pre-malignant to invasive breast cancer regardless of body mass index

50 (BMI)[11]. However, WAT expands via a combination of hyperplasia (increase in adipocyte number) and
51 hypertrophy (increase in adipocyte size)[12], leading to the presence of both small and large cells within obese
52 WAT. Likewise, large adipocytes exist outside of obesity and are especially prevalent in lean individuals with
53 metabolic disorders[13,14]. How small and large adipocytes differ in function, and which effect these changes
54 have on breast cancer cells, remains largely unclear since most studies extrapolate differences by comparing
55 whole tissue isolated from lean and obese donors. However, this approach introduces additional variables
56 (e.g., lipid composition, genetic differences) making it challenging to attribute differences to adipocyte size
57 alone. *In vitro* studies could address these limitations but rely on differentiated progenitor cells which are
58 much smaller in size and functionally distinct compared to primary adipocytes[15]. Thus, improving our
59 understanding of how adipocyte size contributes to tumor progression will require new approaches that
60 enable comparisons of differently sized primary adipocytes isolated from the same WAT depots.
61
62 Studies with primary adipocytes are particularly challenging due, in part, to the distinct properties of these
63 specialized cells. Primary adipocytes are large (often over 100 μm in diameter), buoyant in aqueous media,
64 post-mitotic, and fragile, which renders them incompatible with many culture platforms[16] and single-cell
65 technologies[9]. However, previous experiments using animal models, whole tissue explants, and *in vitro*
66 differentiated progenitor cells implicate adipocytes in breast cancer progression. In particular, adipocytes
67 release pro-inflammatory cytokines which promote tumor cell migration[17], extracellular vesicles which
68 enhance tumor cell proliferation[18], and fatty acids (FAs) which reprogram tumor cell metabolism[19]. Many of
69 these phenomena are exacerbated in obesity, where the endocrine and metabolic functions of adipocytes
70 are impaired[20]. Yet, how altered adipocyte size contributes to these changes remains unclear as we lack the
71 appropriate tools to study primary adipocyte subpopulations of interest in a tractable manner.
72
73 Here, we phenotypically sort primary adipocytes isolated from the same donor into large and small cell
74 populations across both diet-induced and genetic mouse models of obesity. Using RNA sequencing and
75 targeted lipidomics, we characterize inherent phenotypic differences between large and small adipocytes
76 while controlling for other obesity-associated effects. Subsequently, we leverage our recent three-
77 dimensional culture platform[21] to maintain these adipocytes in coculture with breast cancer cells *ex vivo*. We
78 monitor tumor cell lipid accumulation, migration, proliferation, and oxidative metabolism as a function of
79 coculture with different adipocyte subpopulations and assess potential means of intercellular communication
80 which mediated our observations. We then validate the relevance of our findings through our published cohort
81 of human mammary WAT[22] for which banked histology, paired RNA sequencing, and pre-operative blood
82 panels are available. Collectively, our results suggest that adipocyte size independently impacts adipocyte
83 phenotype and, in turn, influences breast cancer progression by altering tumor cell behavior. These findings
84 highlight the potential value of mammary adipocyte size as a prognostic biomarker and point to new
85 therapeutic targets to advance clinical outcomes for women with breast cancer.
86
87 **Results**
88 ***Hypertrophic adipocytes can be isolated by differential buoyancy and size exclusion.***
89 Although adipocyte hypertrophy is a hallmark of obesity, obese WAT contains both large and small adipocytes
90 as it expands through a combination of hyperplasia and hypertrophy (**Fig. 1A**). *In vitro* studies fail to resolve
91 size-dependent differences in adipocyte function due to a reliance on differentiated progenitor cells (**Fig. 1B**),
92 which are multilocular, smaller in size, and functionally distinct compared to primary adipocytes[15]. To address
93 these challenges, we developed experimental strategies to isolate the effect of cell size on adipocyte function
94 while accounting for other covariates associated with weight gain. First, we assessed the size distributions
95 of adipocytes in both diet-induced and genetic mouse models of obesity and their respective lean controls.
96 For diet-induced studies, female C57BL/6 mice were fed a high-fat diet (HFD) or low-fat diet (LFD) for 12
97 weeks starting at 8 weeks of age (**Fig. 1C**). For genetic studies, we used female B6.Cg-Lep[Ob] mice (*ob/ob*)
98 which become morbidly obese due to a loss-of-function mutation in the satiety hormone leptin compared to

99　wild-type (WT) mice[23] (**Fig. 1C**). Consistent with the development of obesity, HFD and *ob/ob* mice weighed
100　significantly more compared to LFD and WT mice at the time of adipocyte isolation (**Fig. S1**). As expected,
101　adipocytes in the mammary fat pads of both HFD and *ob/ob* mice were larger relative to adipocytes in their
102　respective lean controls (**Fig. 1D-E**). Of note, we found that adipocyte hypertrophy was more pronounced in
103　*ob/ob* mice than HFD mice, likely due to the impaired capacity of *ob/ob* progenitor cells to undergo
104　adipogenesis[24]. However, both HFD and *ob/ob* mice contained a broad distribution of cell sizes, including
105　adipocytes similar in size to those found in LFD and WT mice in addition to hypertrophic cells characteristic
106　of obesity. We recognized this inherent heterogeneity as an opportunity to examine the impact of cell size on
107　adipocyte function while controlling for other systemic effects of obesity.
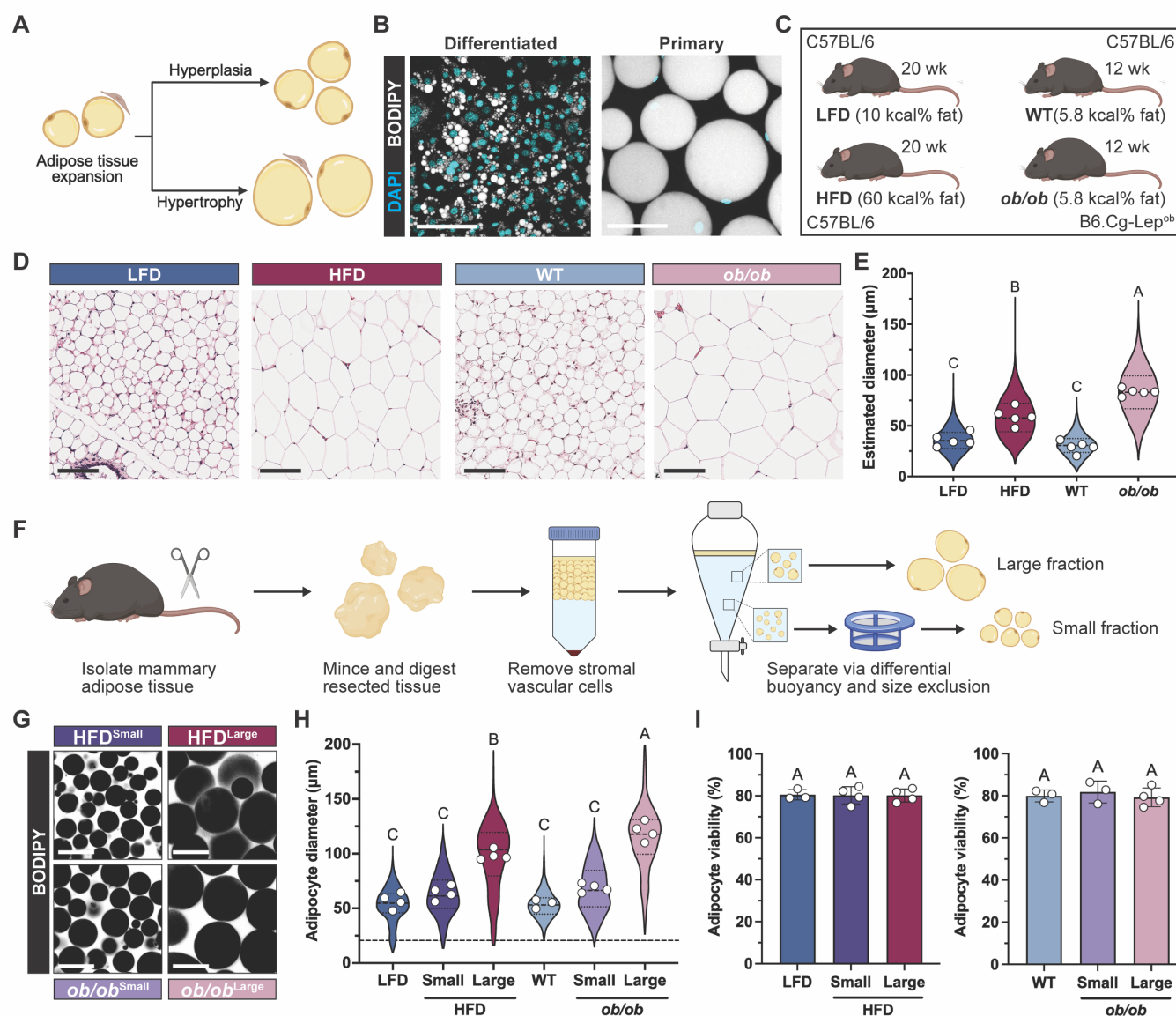
Figure 1. Hypertrophic adipocytes can be isolated by differential buoyancy and size exclusion. (**A**) Schematic of hyperplastic versus hypertrophic adipose tissue expansion. (**B**) Representative images of *in vitro* differentiated and primary adipocytes stained for nuclei (cyan) and neutral lipid (gray). Scale bars = 100 μm. (**C**) Schematic of diet-induced and genetic mouse models of obesity used to isolate primary adipocytes. (**D**) Hematoxylin- and eosin-stained sections of the anterior and inguinal fat pads surrounding the mammary glands of lean and obese mice. Scale bars = 100 μm. (**E**) Quantification of adipocyte diameters estimated from histology. Violin plots show the distribution of all quantified diameters and circles show the average adipocyte diameter per mouse (n = 5). (**F**) Schematic of protocol to separate obese adipocytes by size. (**G**) Representative images of size-sorted adipocytes stained for neutral lipid (gray). Scale bars = 100 μm. (**H**) Quantification of sorted adipocyte diameters. Violin plots show the distribution of all quantified diameters and circles show the average adipocyte diameter per mouse (n = 3–4). Dashed line indicates the average lipid droplet diameter of *in vitro* differentiated adipocytes after two weeks. (**I**) Cell viability of lean and sorted obese adipocytes determined via propidium iodide exclusion (n = 3–4). All data are presented as mean ± standard deviation unless otherwise noted. Statistics were performed with a nested one-way analysis of variance (ANOVA) with Tukey's multiple comparisons test. Compact letter display indicates statistical significance (p = 0.05).

108 To assess the impact of hypertrophy on adipocyte function independently of other obesity-associated
109 changes, we separated adipocytes isolated from HFD and *ob/ob* mice into large and small cells by leveraging
110 size-dependent differences in buoyancy[25] (**Fig. 1F**). Notably, this approach enabled us to obtain small
111 adipocytes from HFD and *ob/ob* mice that were comparable in diameter to adipocytes isolated from LFD and
112 WT mice, respectively (**Fig. 1G-H**). Consistent with histology, large cells from *ob/ob* mice were greater in size
113 than large cells from HFD mice. We also confirmed that size sorting adipocytes from HFD and *ob/ob* mice
114 did not negatively impact cell viability compared to unsorted adipocytes from LFD and WT mice (**Fig. 1I**).
115 Indeed, we maintained viability around 80% for all primary adipocyte subpopulations, consistent with
116 previous results from our lab and others[15,21]. Collectively, these results confirm that we can reliably isolate
117 small and large adipocytes from the mammary fat pads across two independent mouse models of obesity,
118 enabling us to analyze the effect of cell size on adipocyte function independently of other factors.
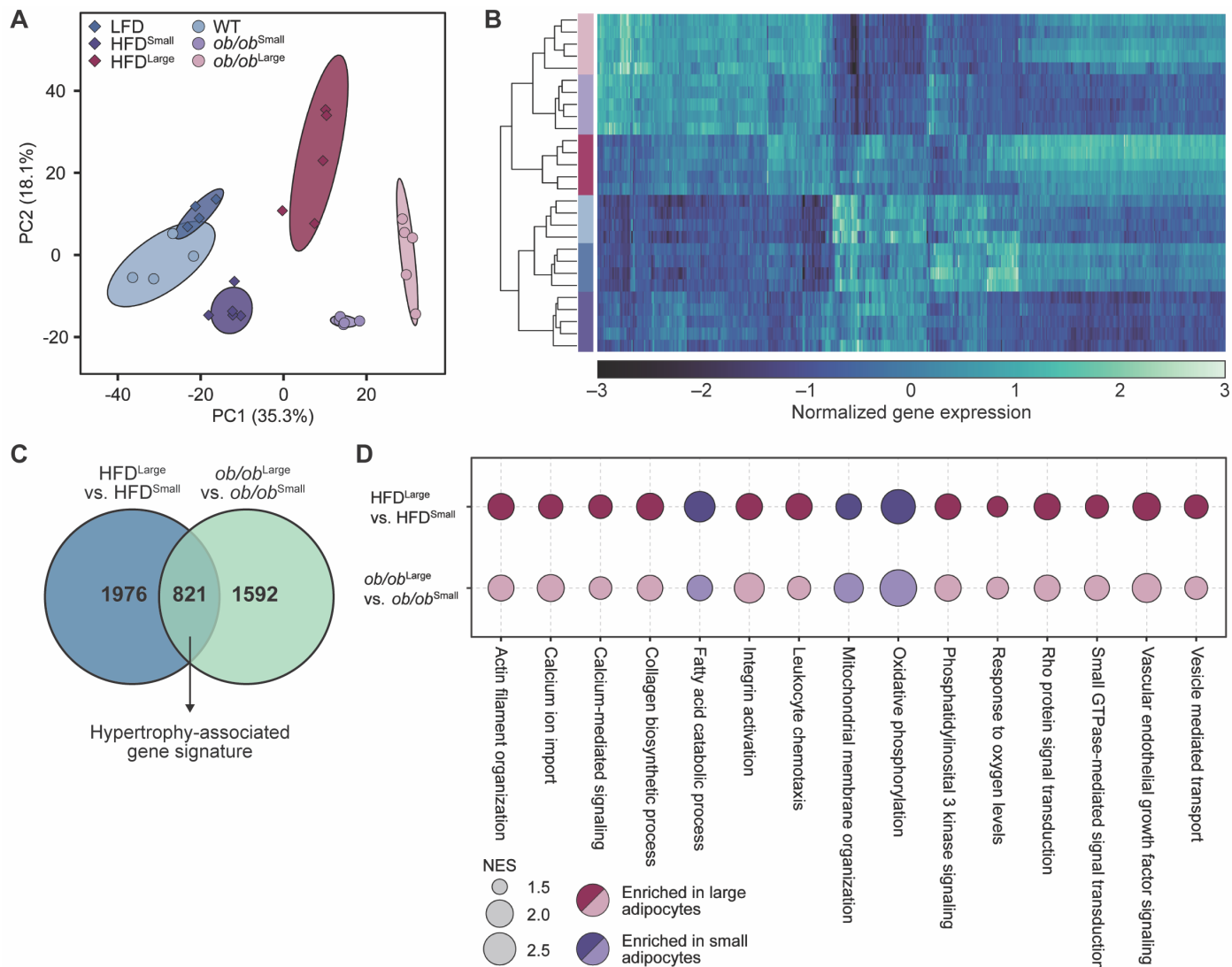
120 ***Large and small adipocytes are transcriptionally distinct.***
121 To broadly assess how size affects adipocyte phenotype, we first performed RNA sequencing on size-sorted
122 adipocytes from HFD and *ob/ob* mice and unsorted adipocytes from LFD and WT mice. Principal component
123 analysis (**Fig. 2A**) and hierarchical clustering (**Fig. 2B**) grouped samples based on condition. For both models
124 of obesity, small adipocytes clustered in between large adipocytes and adipocytes from their respective lean
125 controls, which indicates adipocyte dysfunction in obesity exists along a continuum. Interestingly, small HFD
126 adipocytes clustered more closely to LFD and WT adipocytes than large HFD adipocytes, suggesting that
127 changes to cell size rather than global differences due to diet drive the transcriptional response of adipocytes
128 to obesity. Of note, adipocytes isolated from *ob/ob* mice clustered further away from adipocytes isolated in
129 all other conditions likely due to transcriptional differences driven by global leptin deficiency. Indeed, this
130 result is consistent with sequencing of unsorted adipocytes, which demonstrate a greater number of
131 differentially expressed genes between *ob/ob* and WT adipocytes than HFD and LFD adipocytes (**Fig. S2**).
132 When comparing large and small adipocytes from HFD and *ob/ob* mice, we found a hypertrophy-associated
133 gene signature of 821 differentially expressed genes that were shared across both models of obesity (**Fig.
134 2C**). These results suggest that altered adipocyte size causes distinct transcriptional changes that are
135 independent of how obesity develops (e.g., differences in diet composition for LFD versus HFD mice or
136 genetic differences and quantity of diet consumed for WT versus *ob/ob* mice).

138 Next, we assessed the functional states associated with adipocyte hypertrophy for both obesity models using
139 gene set enrichment analysis (GSEA). Large adipocytes from both HFD and *ob/ob* mice were enriched for
140 gene sets related to adipose tissue dysfunction in obesity[12] including altered collagen deposition, lipid
141 processing, pro-inflammatory signaling, response to hypoxia, and angiogenic signaling (**Fig. 2D**).
142 Interestingly, we also found that large adipocytes were enriched for gene sets related to cytoskeleton
143 organization, calcium- and integrin-mediated mechanosignaling, and RhoA signal transduction, consistent
144 with recent studies indicating that adipocytes mechanically respond to WAT expansion[26–29]. In contrast, small
145 adipocytes were enriched for gene sets related to lipid catabolism, mitochondrial organization, and oxidative
146 phosphorylation, consistent with results linking metabolic syndrome to defective aerobic metabolism in
147 enlarged adipocytes[30,31]. To assess the relevance of our findings in humans, we used our published cohort
148 of 170 mastectomy patients for which banked histology and paired RNA sequencing of uninvolved mammary
149 WAT were available[22] (**Fig. S3A**). We first quantified the mean adipocyte diameter using histology for each
150 patient to compare the transcriptomes of mammary WAT with larger and smaller adipocytes on average (e.g.,
151 patients with adipocyte sizes in the fourth and first quartiles, respectively) (**Fig. S3B-D**). Interestingly, patients
152 in the fourth quartile of mean adipocyte diameter were enriched for similar biological processes from GSEA
153 as large cells across both mouse models of obesity (**Fig. S3E**). Moreover, mammary WAT collected from
154 patients in the fourth quartile of adipocyte diameter was significantly enriched for the hypertrophy-associated
155 gene signature we defined from murine adipocytes (**Fig. S3F**). Collectively, these results indicate that large
156 and small adipocytes are transcriptionally distinct across two mouse models of obesity, that large adipocytes

157   are enriched for gene sets related to WAT dysfunction, and that key transcriptional changes associated with
158   altered adipocyte size are shared between mice and humans.
159

Figure 2. Large and small adipocytes from obese mice are transcriptionally distinct. (**A**) Principal component analysis of gene expression data for lean adipocytes and size-sorted obese adipocytes. Ellipses show the 95% confidence interval for each condition and individual points represent replicates (n = 4–5). (**B**) Heatmap with hierarchical clustering of normalized gene expression data for the top 500 most variable genes between samples. (**C**) Venn diagram of differentially expressed genes (FDR < 0.05) between large and small adipocytes from HFD and *ob/ob* mice, including a hypertrophy-associated gene signature of 821 genes shared across both models. (**D**) Gene sets from Gene Ontology Biological Processes (GOBP) enriched between large and small adipocytes across both models. All comparisons shown meet the criteria set for statistical significance (FDR < 0.05).

160
161   ***Large adipocytes promote breast cancer cell lipid accumulation, migration, and proliferation.***
162   To assess how large versus small adipocytes differentially impact breast cancer cell behavior, we
163   encapsulated size-sorted adipocytes into our recent three-dimensional culture platform as described[21] (**Fig.**
164   **3A**). This approach mimics the collagen-rich extracellular matrix of WAT[32,33] and maintains viability of primary
165   adipocytes in culture for extended periods of time. Moreover, this setup facilitates coculture studies with
166   breast cancer cells by allowing for the exchange of soluble factors between adipocytes and tumor cells while
167   enabling separation of both cell types for downstream analysis. Initial studies with four different breast cancer
168   cell lines and unsorted adipocytes suggested that, regardless of cell line, tumor cells accumulate more lipid
169   when cultured with adipocytes from *ob/ob* relative to WT mice (**Fig. S4**). Of the cell lines tested, MDA-MB-
170   231s acquired the greatest amount of lipid, possibly due to associations between altered lipid metabolism
171   and aggressive mesenchymal cell states[34]. Given these findings, MDA-MB-231s were selected for future
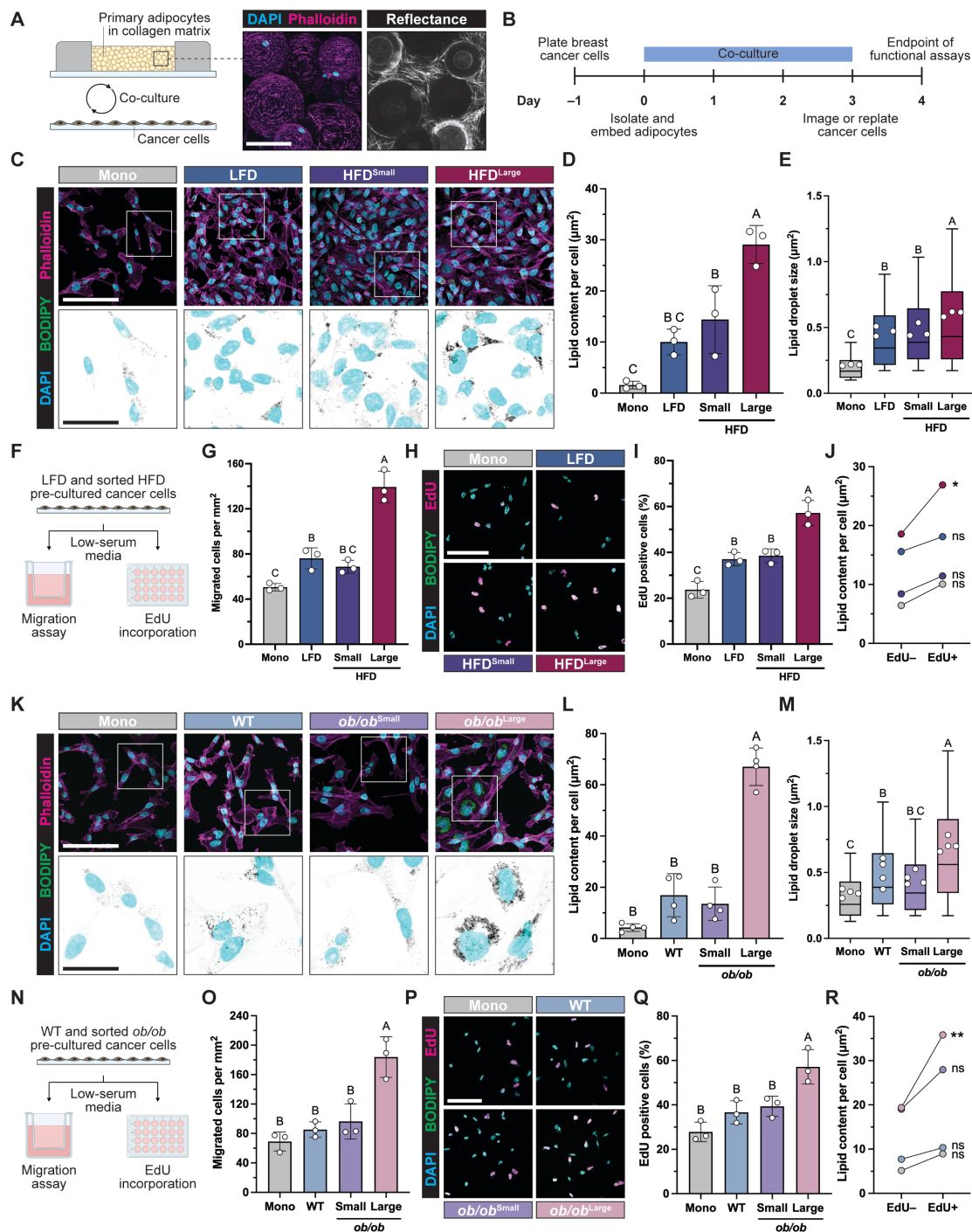
Figure 3. Large adipocytes promote lipid accumulation, migration, and proliferation of breast cancer cells. (**A**) Schematic of coculture setup between primary adipocytes and MDA-MB-231 breast cancer cells with a representative image of adipocytes embedded in collagen stained for nuclei (cyan) and F-actin (magenta). Confocal reflectance image (right) shows collagen fiber structure between cells. Scale bar = 100 μm. (**B**) Timeline of coculture experiments. Representative images of cancer cells after monoculture (mono) or coculture with lean or size-sorted obese adipocytes for diet-induced (**C**) and genetic (**K**) mouse models of obesity. Scale bars = 100 μm. Insets show nuclei (cyan) and neutral lipid (gray). Inset scale bars = 35 μm. Quantification of neutral lipid staining with BODIPY 493/503 per cancer cell for diet-induced (**D**) and genetic (**L**) models (n = 3–4). Size distribution of quantified lipid droplets for diet-induced (**E**) and genetic (**M**) models. Box and whisker plots show the distribution of all droplets and circles show the average droplet size per replicate (n = 3–4). Schematic of migration and proliferation assays of precultured cancer cells for diet-induced (**F**) and genetic (**N**) models. Number of migrated cancer cells 12 hours after reseeding onto a tissue-culture insert for diet-induced (**G**) and genetic (**O**) models (n = 3). Representative images of cancer cells 14 hours after reseeding and 2 hours after EdU treatment for diet-induced (**H**) and genetic (**P**) models. Quantification of EdU-positive cancer cells as a percent of total cells for diet-induced (**I**) and genetic (**Q**) models (n = 3). Average lipid content for EdU– and EdU+ cancer cells across diet-induced (**J**) and genetic (**R**) models (n = 3). All data are presented as mean ± standard deviation unless otherwise noted. Statistics for (J) and (R) performed with a paired t-test per condition. All other statistics performed with a one-way analysis of variance (ANOVA) with Tukey's multiple comparisons test. Compact letter display indicates statistical significance (p = 0.05).

172 studies. To account for differences in adipocyte size reflective of hyperplastic versus hypertrophic expansion,
173 we kept the total volume rather than number of adipocytes constant between conditions. After three days of
174 coculture, MDA-MB-231 breast cancer cells were either fixed and stained for analysis via fluorescence
175 microscopy or reseeded for functional assays (**Fig. 3B**). By staining for neutral lipid with BODIPY 493/503
176 (**Fig. 3C, K**), we found that breast cancer cells cocultured with large adipocytes from HFD or *ob/ob* mice
177 accumulated significantly more lipid than cancer cells cocultured with small adipocytes from HFD or *ob/ob*
178 mice, adipocytes from LFD or WT mice, or monocultured controls (**Fig. 3D, L**). Across both models of obesity,
179 this increase in neutral lipid was due to a greater number of lipid droplets per cell as well as a greater average
180 lipid droplet size (**Fig. 3E, M**), suggesting that large adipocytes promote lipid uptake or biosynthesis by
181 neighboring cancer cells.

183 For functional studies, breast cancer cells precultured with size-sorted adipocytes were reseeded into
184 collagen-coated tissue culture inserts for migration assays or onto glass coverslips for proliferation assays
185 (**Fig. 3F, N**). We found that cancer cells precultured with large adipocytes from HFD or *ob/ob* mice migrated
186 significantly more than cancer cells precultured with small adipocytes from HFD or *ob/ob* mice, adipocytes
187 from LFD or WT mice, or monocultured controls. (**Fig. 3G, O**). Likewise, breast cancer cells precultured with
188 large adipocytes from HFD or *ob/ob* mice were more proliferative relative to all other conditions as measured
189 by incorporation of the thymidine analog 5-ethynyl-2'-deoxyuridine (EdU) (**Fig. 3H-I, P-Q**). Interestingly, EdU-
190 positive cancer cells had more lipid than EdU-negative cancer cells on average across all conditions, but this
191 difference was most pronounced and only statistically significant for breast cancer cells precultured with large
192 adipocytes from HFD or *ob/ob* mice (**Fig. 3J, R**). These results suggest that increased cancer cell proliferation
193 due to preculture with large adipocytes may be mediated by the greater presence of lipid in these cells, and
194 we aimed to test this hypothesis moving forward. Collectively, our findings indicate that soluble factors
195 released by large versus small adipocytes promote breast cancer cell lipid accumulation, as well as migration
196 and proliferation. Since we observed similar trends between experiments performed with HFD and *ob/ob*
197 mice, we focused our remaining studies on adipocytes isolated from *ob/ob* mice given that these mice do not
198 require expensive and lengthy feeding periods prior to tissue isolation.

200 ***Large adipocytes alter breast cancer cell lipid metabolism.***
201 Given that adipocytes are implicated in altering lipid metabolism in melanoma cells[35,36] and that we observed
202 adipocyte size positively correlated with lipid accumulation in cocultured breast cancer cells (**Fig. 3D, L**), we
203 speculated that adipocyte size promoted tumor cell migration and proliferation in our studies by affecting lipid
204 metabolism. Interestingly, fluorescence staining revealed that lipid droplets were closely associated with the
205 mitochondrial network of MDA-MB-231 breast cancer cells cocultured with adipocytes (**Fig. 4A**), suggestive
206 of altered lipid metabolism given that FAs must be transported from cytoplasmic lipid droplets into the
207 mitochondria to generate ATP via a process known as FA oxidation (FAO). To test this possibility, we first
208 measured the oxygen consumption rate of breast cancer cells precultured with different adipocyte
209 populations as a relative metric of mitochondrial activity in the presence or absence of etomoxir, which
210 prevents FAO by irreversibly inhibiting carnitine palmitoyltransferase-1 (CPT1A) and precluding the transport
211 of FAs into the mitochondria (**Fig. 4B**). At baseline, breast cancer cells precultured with large *ob/ob*
212 adipocytes consumed more oxygen per ng of DNA than those precultured with small *ob/ob* adipocytes, WT
213 adipocytes, or monocultured controls as determined by metabolic flux analysis (**Fig. 4C**). Treatment with
214 etomoxir reduced oxygen consumption rates for all precultured conditions to levels comparable to
215 monocultured controls for both basal respiration (**Fig. 4D**) and maximal respiration (**Fig. 4E**), which was
216 induced by the addition of the electron transport chain uncoupler FCCP. However, etomoxir had the greatest
217 relative effect on MDA-MB-231 cells that were precultured with large *ob/ob* adipocytes. These results indicate
218 that cell-cell communication between large adipocytes and breast cancer cells increases tumor cell oxygen
219 consumption in a manner dependent on the oxidation of FAs as metabolic substrates. To determine if this
220 increased mitochondrial activity was responsible for our observed changes in breast cancer cell behavior in

221 our previous preculture studies, we repeated these experiments but treated cancer cells with or without
222 etomoxir when replating for functional assays (**Fig. 4F**). Strikingly, the addition of etomoxir prevented
223 increases to MDA-MB-231 migration (**Fig. 4G**) and proliferation (**Fig. 4H**) following preculture with large *ob/ob*
224 adipocytes compared to vehicle controls. Etomoxir treatment also negated the correlation between lipid
225 content and EdU incorporation (**Fig. 4I**), which suggests that an inability to use FAs as metabolic substrates
226 prevents the growth advantage otherwise conferred to breast cancer cells with greater lipid accumulation.
227 Collectively, our results indicate that large adipocytes secrete factors which increase the mitochondrial
228 activity of breast cancer cells by promoting FAO and, in turn, facilitating their migration and proliferation.
229
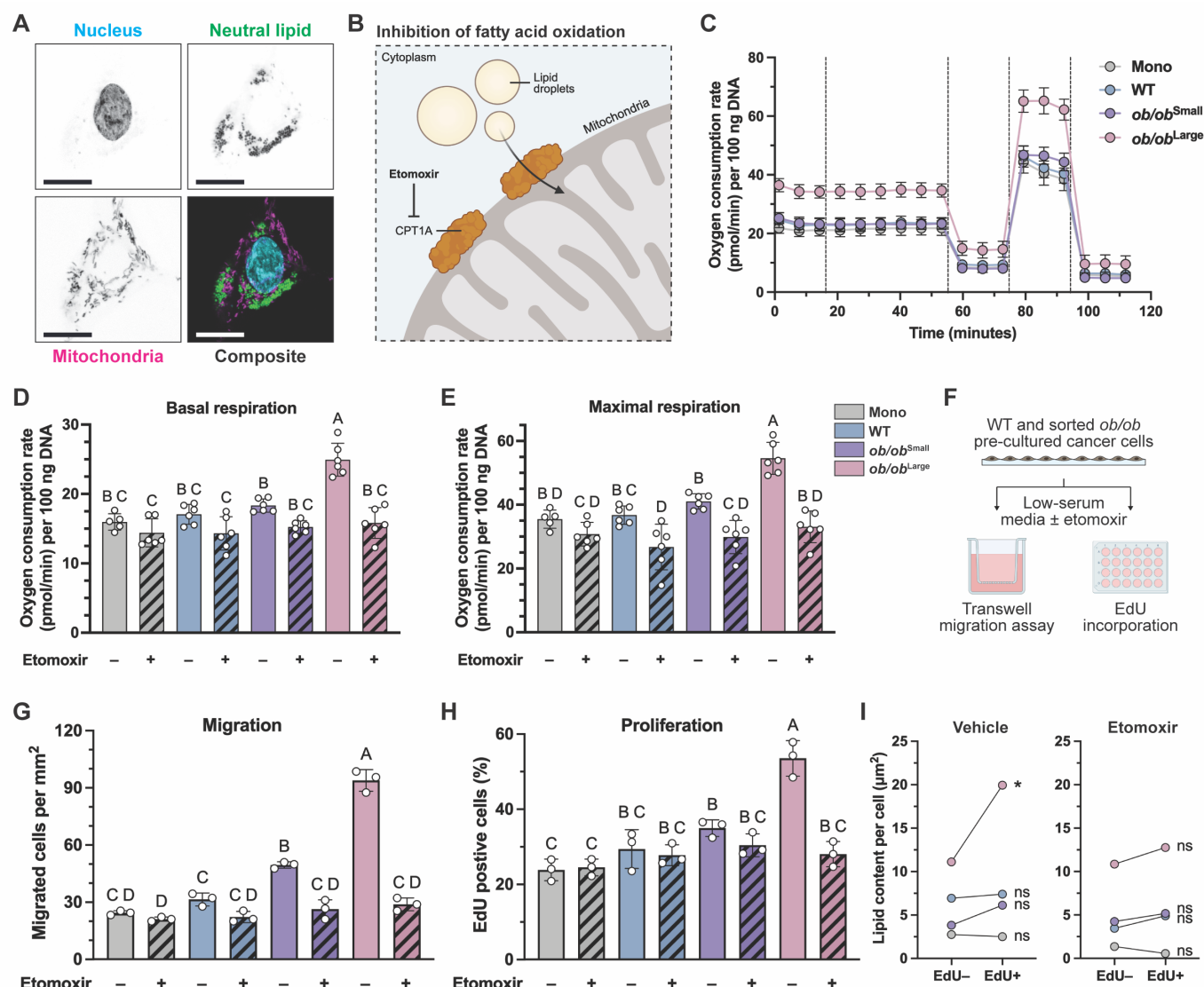
Figure 4. Large adipocytes alter breast cancer cell lipid metabolism to promote migration and proliferation. (**A**) Representative image of a precultured MDA-MB-231 breast cancer cell showing colocalization of neutral lipid and mitochondria. Scale bar = 15 µm. (**B**) Schematic of FAO inhibition by etomoxir. (**C**) Normalized oxygen consumption rate of monocultured or precultured cancer cells over time. Dashed lines indicate sequential addition of etomoxir or vehicle, oligomycin, FCCP, and rotenone/antimycin A (n = 5–6). Only vehicle conditions are plotted to improve visibility. (**D**) Quantification of basal respiration rate per condition from (C) (n = 5–6). (**E**) Quantification of maximal respiration rate per condition from (C) (n = 5–6). (**F**) Schematic of migration and proliferation assays for precultured cancer cells treated with etomoxir or vehicle control. (**G**) Number of migrated cancer cells 12 hours after reseeding onto a tissue-culture insert with or without etomoxir (n = 3). (**H**) Quantification of EdU-positive cancer cells as a percent of total cells with or without etomoxir (n = 3). (**I**) Average lipid content for EdU– and EdU+ cancer cells across conditions (n = 3). All data are presented as mean ± standard deviation unless otherwise noted. Statistics for (I) performed with a paired t-test per condition. All other statistics performed with a one-way analysis of variance (ANOVA) with Tukey's multiple comparisons test. Compact letter display indicates statistical significance (p = 0.05).

230

Large adipocytes increase lipid transfer via vesicle-mediated release.

We next aimed to assess if the increased lipid content of breast cancer cells cocultured with large adipocytes could be due to size-dependent differences in lipid release. To first confirm that cancer cells uptake lipid released by adipocytes, we pre-labeled adipocytes with BODIPY 493/503 prior to coculture. After 48 hours, we observed the presence of pre-labeled, adipocyte-derived lipid in cocultured breast cancer cells (**Fig. 5A**). These results suggested that adipocytes increase the lipid content of cocultured cancer cells via direct transfer of lipid rather than by changing tumor cell lipogenesis. We then aimed to determine how large adipocytes increase lipid transfer given that adipocytes can release lipids via two separate mechanisms. Canonical lipolysis by adipocytes is mediated by lipase-dependent breakdown of triglycerides into glycerol and non-esterified FAs, which then bind to carrier proteins for export into the extracellular space (**Fig. 5Bi**). In addition, adipocytes can release lipid via a lipase-independent mechanism where small lipid droplets containing intact triglycerides bud from the central lipid droplet and are packaged into extracellular vesicles for secretion[37] (**Fig. 5Bii**). Conversely, cancer cells store triglycerides in their own lipid droplets, which requires esterification of FAs following uptake or lipogenesis (**Fig. 5C**). To determine which of these two mechanisms facilitates increased accumulation of lipid in breast cancer cells due to coculture with large adipocytes, we first measured the glycerol content of media collected from our coculture experiments as a relative metric of lipolysis. Media collected from cocultures of cancer cells with large *ob/ob* adipocytes contained less glycerol than cocultures with small *ob/ob* or WT adipocytes (**Fig. 5D**). These results suggest that the rate of lipolysis, as estimated by glycerol release, cannot explain the observed increase in lipid content of cancer cells cocultured with large adipocytes. Therefore, we next tested whether adipocytes transfer lipid to cancer cells via extracellular vesicles and if this transfer differs as a function of adipocyte size. To this end, we purified extracellular vesicles from the media of a constant volume of small or large adipocytes in monoculture via ultracentrifugation for downstream analysis (**Fig. 5E**). We found that large *ob/ob* adipocytes secreted significantly more vesicles than small *ob/ob* or WT adipocytes (**Fig. 5F**). This increase was primarily driven by vesicles less than 200 nm in size, suggestive of greater exosome release (**Fig. 5G**). Moreover, we confirmed the purity of our isolated vesicles by blotting for the cell-specific marker FAK the general extracellular vesicle marker FLOT2 (**Fig. 5H**). We then validated these results with adipocytes isolated from HFD and LFD mice. Similarly, we found that media from cocultures of cancer cells with large HFD adipocytes contained less glycerol than other conditions and that large HFD adipocytes secreted significantly more vesicles per cell volume than small HFD or LFD adipocytes (**Fig. S5**).

To determine if adipocytes of varying size differed in their lipid composition, which could, in turn, influence lipid accumulation in cocultured breast cancer cells, we performed targeted lipidomics of total and non-esterified FAs in WT, small *ob/ob*, and large *ob/ob* adipocytes (**Fig. 5I**). While large *ob/ob* adipocytes contained more saturated, unsaturated, and total FAs per mg protein relative to small *ob/ob* and WT adipocytes as expected, we did not observe consistent differences in the relative composition of specific lipid species in small versus large *ob/ob* adipocytes (**Fig. S6-S7**). However, both small and large *ob/ob* adipocytes contained a higher ratio of arachidonic acid to eicosapentaenoic and docosahexaenoic acids than WT adipocytes, indicative of a pro-inflammatory lipid profile and suggestive of altered FA desaturase activity in *ob/ob* adipocytes given that *ob/ob* and WT mice received the same diet (**Fig. S6-S7**). These results underscore the importance of examining adipocytes from the same donor when investigating the impact of size on adipocyte function, as some differences in adipocyte phenotype are donor-dependent regardless of size. Interestingly, we found that the percentage of non-esterified to total FAs was significantly decreased in large versus small *ob/ob* adipocytes (**Fig. 5J**), consistent with our glycerol release data that large cells are less lipolytic relative to small cells. Finally, to confirm that the increased lipid content of cancer cells cocultured with large versus small *ob/ob* adipocytes was due to vesicle-mediated transfer, we applied extracellular vesicles collected and purified from a constant volume of size-sorted adipocytes in monoculture to cancer cells in monoculture. Moreover, we inhibited DGAT-1 and DGAT-2 (iDGAT) concurrently with vesicle treatment in a subset of samples to prevent esterification of free FAs and further rule out the contributions of
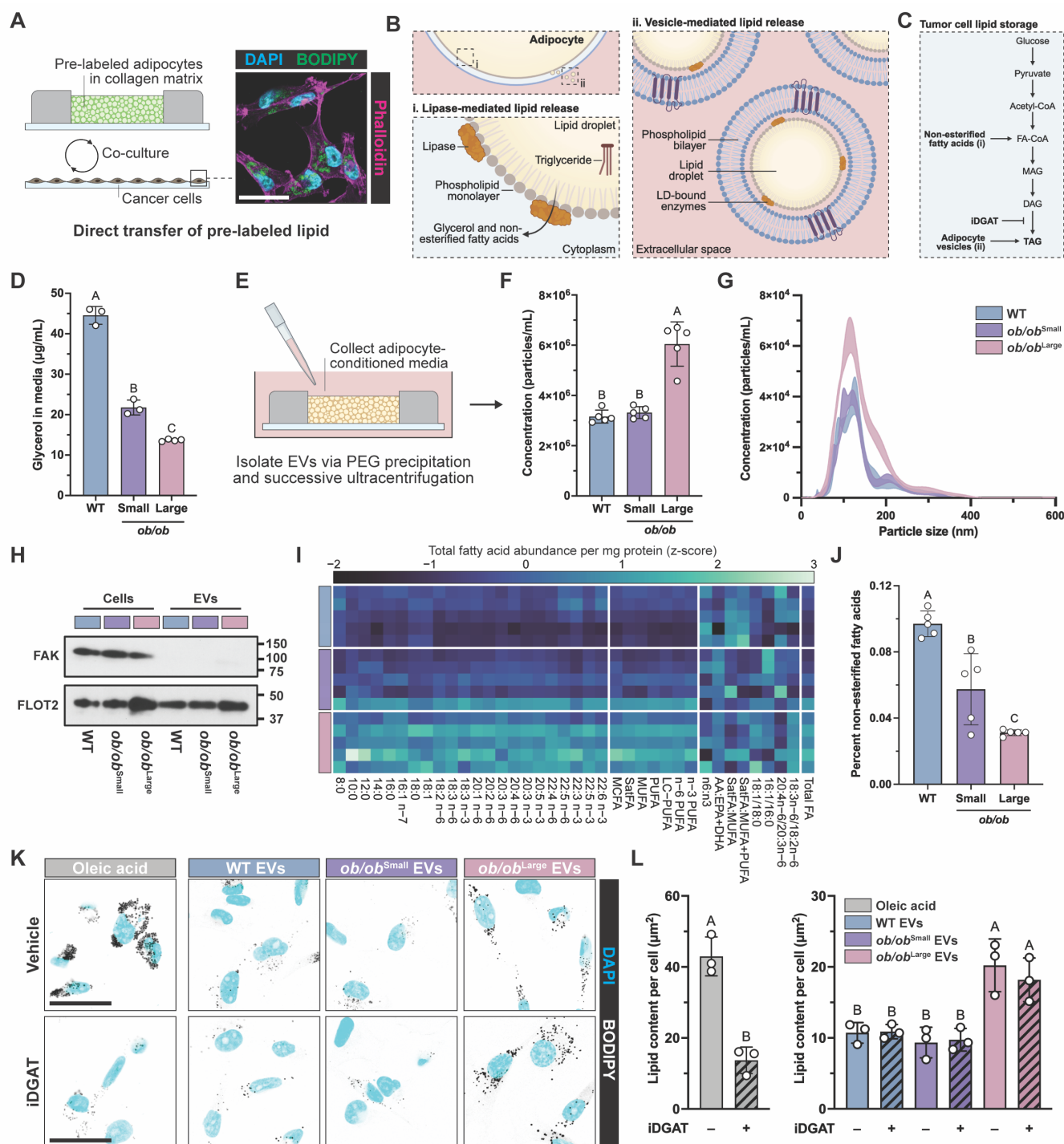
Figure 5. Large adipocytes promote breast cancer cell lipid accumulation through extracellular vesicle-mediated transfer of triglycerides. (**A**) Schematic of lipid transfer experiment. Adipocytes were pre-labeled with BODIPY 493/503 and washed to remove excess dye prior to the initiation of coculture. Scale bar = 35 μm. (**B**) Schematic of lipase-mediated (i) and vesicle-mediated (ii) lipid release by adipocytes. (**C**) Schematic of lipid storage by cancer cells. (**D**) Concentration of glycerol in conditioned media collected from cancer cells and adipocytes in coculture after 72 hours (n = 3–4). (**E**) Schematic of extracellular vesicle isolation from adipocyte-conditioned media. (**F**) Concentration of extracellular vesicles collected from adipocytes in monoculture after 24 hours (n = 5). (**G**) Size distribution of extracellular vesicles from (F) (n = 5). (**H**) Western blot of cell and extracellular vesicle lysates collected from lean and size-sorted obese adipocytes. (**I**) Heatmap of targeted lipidomics data showing the total FA composition of lean and size-sorted obese adipocytes normalized to protein content (n = 5). (**J**) Percent of non-esterified relative to total FAs from (I) (n = 5). (**K**) Representative images of MDA-MB-231 breast cancer cells 24 hours after treatment with oleic acid as a positive control or extracellular vesicles collected from WT, small *ob/ob*, or large *ob/ob* adipocytes. Cancer cells were also treated concurrently with vehicle or dual inhibitors for DGAT-1 and DGAT-2 (iDGAT). Scale bars = 35 μm. (**L**) Quantification of neutral lipid staining with BODIPY 493/503 from (K) per cancer cell (n = 4). All data are presented as mean ± standard deviation unless otherwise noted. Statistics were performed with a one-way analysis of variance (ANOVA) with Tukey's multiple comparisons test. Compact letter display indicates statistical significance (p = 0.05).

280 lipogenesis by cancer cells (**Fig. 5C**). After 24 hours, we found that breast cancer cells treated with vesicles
281 from large *ob/ob* adipocytes contained significantly more lipid than those treated with vesicles from small
282 *ob/ob* or WT adipocytes (**Fig. 5K-L**). However, lipid uptake was significantly lower across all conditions
283 compared to coculture studies, likely due to the shorter period of vesicle collection (24 hours) than coculture
284 (72 hours) and loss of vesicles during sample processing. Nevertheless, iDGAT prevented lipid storage in
285 tumor cells treated with exogenous oleic acid as expected, while iDGAT treatment did not affect lipid transfer
286 via adipocyte-derived vesicles (**Fig. 5K-L**), indicating that these vesicles contain intact triglycerides rather
287 than non-esterified FAs and that altered lipogenesis does not significantly contribute to cancer cell lipid
288 content in our coculture system. Collectively, our results indicate that large adipocytes promote breast cancer
289 cell lipid uptake through vesicle-mediated transfer of intact triglycerides.
290
291 ***Adipocyte size is more predictive of lipid dysfunction than body mass index.***
292 Given that we observed greater lipid release by large adipocytes in our coculture studies, we next aimed to
293 determine if adipocyte size correlated with broader, systemic metabolic changes in humans. To this end, we
294 compared banked adipose tissue and pre-operative blood panels for each of the 170 mastectomy patients
295 in our cohort (**Fig. 6A**). Again, we stratified patients into quartiles based on their average adipocyte diameter
296 determined via paired histology (**Fig. 6B**). Using this approach, we found that average adipocyte diameter
297 (**Fig. 6C**) more accurately stratified patients diagnosed with dyslipidemia than BMI category (**Fig. 6D**).
298 Likewise, average adipocyte diameter correlated more significantly with fasting triglycerides (**Fig. 6E**) than
299 BMI (**Fig. 6F**), even when their interaction effects were considered using multiple linear regression (**Fig. 6G**).
300 Collectively, these findings suggest that in addition to releasing more lipid to cells locally, as observed in our
301 coculture studies, large adipocytes may also increase lipid release into circulation with consequences for
302 whole-body metabolism.
303
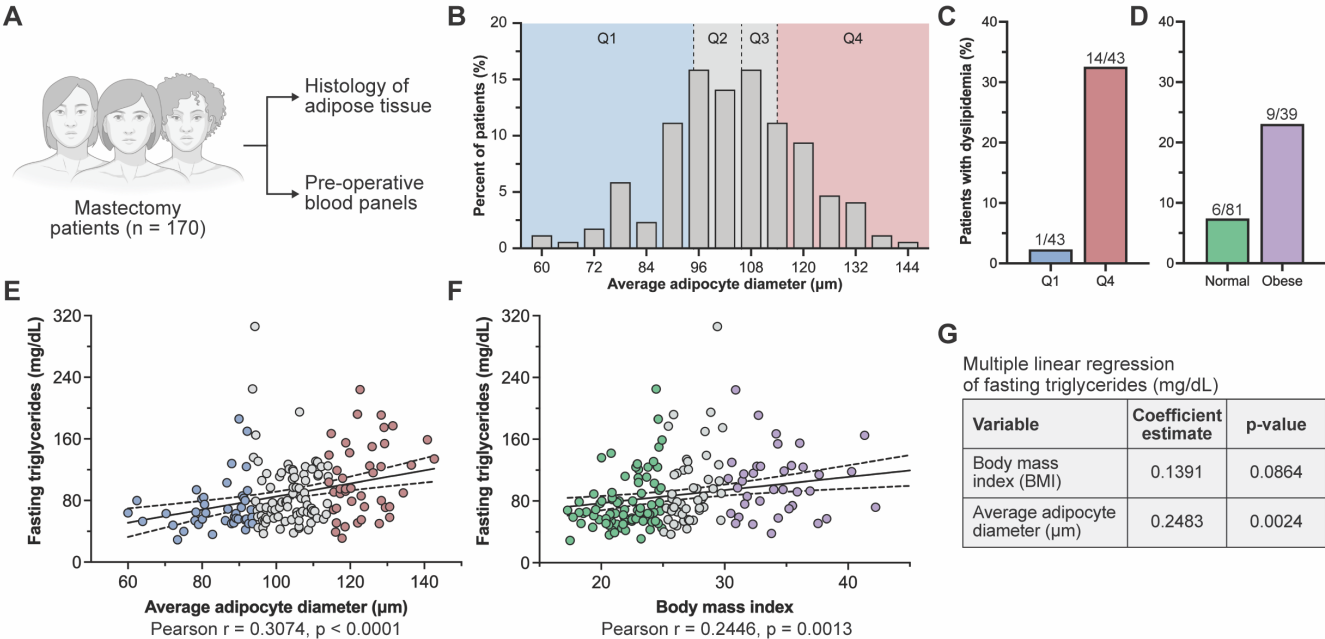
Figure 6. Adipocyte size is more predictive of systemic lipid dysfunction than body mass index. (**A**) Schematic of paired mammary adipose tissue histology and pre-operative blood panels from a cohort of 170 mastectomy patients. (**B**) Histogram of patients stratified into quartiles based on their average adipocyte diameter determined from histology. Percent of patients diagnosed with dyslipidemia when classified by (**C**) average adipocyte diameter or (**D**) BMI category (BMI < 25 for normal, BMI > 30 for obese). Simple linear regression of fasting triglycerides versus (**E**) average adipocyte diameter or (**F**) BMI. (**G**) Multiple linear regression of fasting triglycerides as a function of both average adipocyte diameter and BMI following z-score normalization.

304

Discussion

Obesity is an established risk factor for breast cancer initiation and prognosis but the mechanisms behind these associations remain unclear. Our results suggest that the increased presence of hypertrophic adipocytes in obese WAT contributes to these observations and that adipocyte size could serve as a more specific prognostic biomarker than BMI for breast cancer patients. In particular, we find that large adipocytes are transcriptionally distinct from small adipocytes isolated from donor-matched tissue and increase lipid accumulation in neighboring breast cancer cells through vesicle-mediated release of triglycerides. In turn, coculture with large adipocytes enhances breast cancer cell migration, proliferation, and oxygen consumption in a manner dependent on FAO. Collectively, our findings suggest that examining mammary WAT morphology during breast cancer biopsy could help identify women at greatest risk for aggressive disease and regions of tissue most susceptible to invasion.

Our understanding of adipocyte heterogeneity and biology remains limited given that single-cell analysis of primary cells is challenging due to their buoyancy and fragility[9,16]. Here, we sequenced adipocytes phenotypically sorted by size and identified that large, hypertrophic adipocytes constitute a transcriptionally distinct subpopulation of cells. Our findings are consistent with recent results demonstrating that WAT is more plastic[7,8] and heterogenous[9,10] than once considered. For example, multiple adipocyte subpopulations have been identified in mice with distinct sensitivities to insulin[10] and whose relative proportions change with administration of a high-fat diet[9]. In our data, large adipocytes from both diet-induced and genetic mouse models of obesity were enriched for gene sets related to WAT dysfunction[12], as were tissue samples collected from mastectomy patients with increased adipocyte size regardless of BMI. Moreover, large adipocytes also exhibited enrichment for gene sets related to collagen deposition, actin cytoskeleton remodeling, calcium ion transport, and Rho protein signal transduction, consistent with an emerging understanding of the mechanoresponsive adaptations required of adipocytes during drastic cell expansion[27,29]. To what extent these transcriptional changes are adipocyte intrinsic or a function of environmental cues in hypertrophic regions of WAT remains to be determined. Re-examining the transcriptome of large adipocytes after extended *ex vivo* culture could help make this distinction. Likewise, assessing hypertrophic adipocytes in the absence of obesity, such as those present in lean individuals with metabolic disorders[13], could help identify the relative contribution of cell intrinsic factors. Regardless of the cause, our findings underscore the need for a more nuanced view of WAT beyond BMI that accounts for other prognostic parameters such as adipocyte size. Indeed, in blood panels collected from our cohort of mastectomy patients, average adipocyte diameter correlated more significantly with dyslipidemia and fasting triglycerides than BMI, even when their interaction effects were considered—findings that are broadly consistent with the increased release of lipid by large adipocytes in our coculture experiments.

Previous studies have demonstrated that adipocytes can influence the behavior of neighboring tumor cells, though this connection is most established for melanoma as opposed to other carcinomas that develop in WAT-rich stroma such as breast cancer. For example, researchers found that melanoma cells overexpress fatty acid transport protein 1 (FATP1), which facilitates the uptake of adipocyte-derived non-esterified FAs and promotes tumor invasion[36]. In a separate study, adipocyte-derived exosomes, which were enriched for proteins implicated in FAO, mediated the metabolic reprogramming of melanoma cells[35]. In the context of breast cancer, several studies have linked adipocyte-derived lipids to altered tumor cell metabolism[19,38]. However, these studies used *in vitro* differentiated progenitor cells and thus did not assess obesity- or hypertrophy-dependent effects. Indeed, while we saw trends for cocultures with small adipocytes, we only observed significant changes in breast cancer cell phenotypes (i.e. lipid content, migration, proliferation, oxygen consumption) for cocultures with large adipocytes. This may be due to our experimental setup, as we performed shorter cocultures than some of the cited studies[19,36] or may reflect underlying differences in adipocyte-tumor cell communication when using primary adipocytes. Moreover, our results corroborate previous findings that obese WAT secretes more extracellular vesicles per mg tissue than lean WAT[37] and

354   that this increase is driven by adipocytes rather than cells of the stromal vascular fraction[35]. Our findings
355   indicate that the greater rate of extracellular vesicle release by obese WAT likely stems from the increased
356   presence of hypertrophic adipocytes in obesity, a conclusion not previously possible with gross analysis of
357   tissue explants or unsorted cells. Moving forward, future studies will be needed to assess the impact of these
358   adipocyte-derived vesicles on other breast cancer subtypes and stromal cells, such as tissue-resident
359   macrophages and fibroblasts, within the breast cancer microenvironment.
360
361   Across experiments, our findings suggest that large adipocytes shift toward favoring a vesicle-mediated
362   mode of lipid release, though the lack of endocrine signals which stimulate lipolysis in our system may be a
363   confounding factor in these observations. Indeed, across both mouse and human sequencing data,
364   hypertrophic adipocytes and hypertrophic WAT demonstrated positive gene set enrichment for vesicle-
365   mediated transport and negative gene set enrichment for lipid catabolism. While initially counterintuitive given
366   the greater degree of lipid transfer observed between large adipocytes and breast cancer cells in coculture,
367   these findings are consistent with a lipase-independent, vesicle-mediated mode of lipid release by
368   hypertrophic cells. Direct transfer of adipocyte-derived triglycerides via extracellular vesicles as opposed to
369   non-esterified FAs via lipolysis could offer several potential advantages to recipient tumor cells. Beyond
370   serving as metabolic substrates for FAO, a steady supply of vesicle-delivered triglycerides may also provide
371   a readily available source of FAs for membrane biosynthesis, lipid signaling, and intracellular trafficking. In
372   particular, tumor cells undergoing rapid division exhibit increased demand for phospholipids to sustain
373   plasma membrane expansion, and specific lipid classes such as monounsaturated and polyunsaturated FAs
374   are necessary for membrane fluidity and lipid raft formation[39]. Our lipidomics data indicate that large
375   adipocytes contain an increased abundance of these classes of FAs relative to small adipocytes. This finding
376   suggests that vesicle-mediated lipid transfer could facilitate tumor progression not only by fueling oxidative
377   metabolism but also by supplying key structural lipids for tumor growth. Future untargeted lipidomics of the
378   specific lipid species enriched in adipocyte-derived vesicles, as well as the lipids transferred to recipient
379   tumor cells, will be critical to dissect this potential dual role of FAs in breast cancer malignancy.
380
381   In addition to triglycerides, previous studies have demonstrated that extracellular vesicles secreted by
382   adipocytes are also enriched for lipid-droplet-associated proteins required for FAO[35,37]. Thus, by increasing
383   vesicle release, hypertrophic adipocytes may provide tumor cells not only with FAs for mitochondrial oxidation
384   but also the molecular machinery needed to metabolize them. Future proteomic studies of vesicles derived
385   from large versus small adipocytes would reveal if altered protein cargo contributed to our observed increase
386   in FAO for breast cancer cells precultured with large adipocytes. Moreover, excess quantities of non-esterified
387   FAs, especially trans- or saturated FAs, can induce lipotoxicity by activating cell stress responses[40]. Indeed,
388   inhibiting the ability of tumor cells to esterify free FAs, and thus induce lipotoxicity, has been explored as a
389   therapeutic strategy for hepatocellular carcinoma[41]. In contrast, the direct transfer of intact triglycerides would
390   bypass the need for FA esterification and limit the potential lipotoxic effects on cancer cells. Conversely,
391   controlled oxidation of FAs by tumor cells has been shown to mediate chemoresistance to platinating
392   agents[42], which are increasingly prescribed for patients with advanced or triple-negative breast cancer[43].
393   Thus, moving forward, the effect of specific adipocyte populations of interest on breast cancer
394   chemoresistance should be explored. More broadly, this shift in the mode of lipid release by hypertrophic
395   adipocytes likely produces systemic metabolic alterations outside the context of cancer by altering the
396   bioavailability and biodistribution of lipids in circulation, as supported by our patient data.
397
398   In conclusion, our results suggest that the increased presence of hypertrophic adipocytes in mammary WAT
399   for obese women with breast cancer contributes to the poor clinical outcomes seen in these patients.
400   However, risk stratification by BMI alone is a flawed approach given that not all WAT expands equally. Indeed,
401   our findings posit that adipocyte size could serve as an independent prognostic biomarker for breast cancer
402   patients regardless of BMI. Determining adipocyte size is clinically tractable given that peritumoral WAT is

403   often included in routine biopsies used for diagnosis and automated approaches exist to characterize

404   adipocyte morphology[44,45]. Moreover, our results emphasize that strategies to interfere with tumor cell lipid

405   uptake or metabolism could provide new therapeutic avenues for patients with hypertrophic WAT at their

406   tumor margins. Collectively, our findings provide critical insight into the role of hypertrophic adipocytes as a

407   distinct cell population with implications for the management of breast cancer and metabolic diseases more

408   broadly.

Acknowledgments

Author contributions

G.F.B. and C.F. conceived and designed experiments. G.F.B. performed all experiments with assistance from M.I.P. unless otherwise noted. R.R.V. and M.C.R. performed targeted lipidomics and associated analysis. M.A.A. performed Western blotting of cell and extracellular vesicle lysates. D.D.G., D.J.F., and N.M.I. obtained and analyzed the cohort of human mammary adipose tissue collected from mastectomy patients. G.F.B. prepared all figures and schematics. G.F.B. and C.F. wrote the manuscript with input from all authors.

Data and code availability

All source data and code will be provided in the final publication of this manuscript.

Competing interests

The authors declare no competing interests.

Materials and methods

Culture of breast cancer cell lines

MDA-MB-231, MCF7, PY8119, and EO771 breast cancer cell lines were maintained in high-glucose Dulbecco's Modified Eagle Medium (Gibco #12800) supplemented with 10% (v/v) fetal bovine serum (FBS, R&D Systems #S11150) and 1% (v/v) penicillin-streptomycin (ThermoFisher #15070063) unless otherwise noted. Primary adipocytes and cocultures were maintained in a 1:1 mixture of low-glucose Dulbecco's Modified Eagle Medium (Gibco #316000) and Ham's F12 Nutrient Mix (Gibco #21700) supplemented with 10% (v/v) FBS and 1% (v/v) penicillin-streptomycin unless otherwise noted. For functional studies of precultured tumor cells, a 1:1 mixture of low-glucose Dulbecco's Modified Eagle Medium and Ham's F12 Nutrient Mix supplemented with 1% (v/v) FBS and 1% (v/v) penicillin-streptomycin was used. For experiments involving extracellular vesicle collection or treatment, exosome-depleted FBS (ThermoFisher #A2720803) was used to limit the presence of exogenous vesicles.

Maintenance and differentiation of 3T3-L1 preadipocytes

Prior to the induction of adipogenesis, 3T3-L1s were seeded at a density of 5,000 cells per cm^2 onto 12 mm glass coverslips coated with 30 µg/mL collagen type I (VWR #47747-218) and cultured until 80% confluent. Adipogenesis was initiated with induction media consisting of high-glucose DMEM supplemented with 5% FBS, 1% penicillin-streptomycin, 1 mM dexamethasone (Sigma-Aldrich #D4902), 500 mM IBMX (Krackeler Scientific #45-I7018), 20 mM indomethacin (Sigma-Aldrich #405268), and 200 µM insulin (Krackeler Scientific #45-91077C). After 48 hours, cells were changed to maintenance media consisting of high-glucose DMEM supplemented with 5% FBS, 1% penicillin-streptomycin, and 200 µM insulin. Maintenance media was replaced every 48 hours until experimental endpoints were reached.

Animal models

For all animal studies, WAT was isolated from the anterior and inguinal fat pads around the mammary glands of nulliparous female C57BL6 mice (The Jackson Laboratories). For the genetic model of obesity, wildtype C57BL6 mice (strain 000664) and leptin-deficient B6.Cg-Lep[ob] mice (strain 000632) were purchased at 10 weeks of age and fed a standard rodent diet (LabDiet #5053) *ad libitum* until sacrifice at 12 weeks of age. For the dietary model of obesity, wildtype C57BL6 mice were purchased at 6 weeks of age and fed a standard rodent diet for a two-week acclimation period. At 8 weeks of age, mice were randomized and placed on either a low-fat diet (Research Diets #D12450J, 10 kcal% fat) or high-fat diet (Research Diets #D12492, 60 kcal% fat) *ad libitum* until sacrifice at 20 weeks of age. Diets were administered weekly and remaining chow from the previous week was discarded. All mice were housed between 21°C and 23°C. All animal protocols were approved by the Institutional Animal Care and Use Committees at Weill Cornell Medicine and Cornell University.

Histology of resected adipose tissue

Pieces of resected WAT were collected from euthanized C57BL6 mice and fixed in 4% (w/v) paraformaldehyde in 1x PBS for 24 hours at 4°C. Resected tissue was then stored in 70% (v/v) ethanol in water at 4°C until processing. Samples were sent to the Cornell College of Veterinary Medicine Animal Health Diagnostic Center for paraffin embedding, sectioning, and staining with hematoxylin and eosin. Stained sections were imaged and digitized on an Aperio ScanScope CS2 (Leica) with a 40x objective.

Primary adipocyte isolation

Resected WAT was immediately placed in cold DMEM/F12 until processing. Tissue was then minced for several minutes until separated into approximately 1 mm^3 pieces. Floating tissue pieces were decanted and reserved while any remaining pieces were discarded. The reserved tissue was then digested in 1.5 mg/mL collagenase type I (Worthington Biochemical #LS004197) in Hank's Buffered Salt Solution (Gibco #14065056) supplemented with 1% (w/v) bovine serum albumin (ThermoFisher #BP1600-100) in a vertical

485 tube rotator for 50 minutes at 37°C. The resulting cell suspension was passed through 200 µm cell strainers
486 (pluriSelect #435020003) to remove undigested pieces of tissue. Adipocytes were allowed to float out of
487 solution for 10 minutes before the infranatant was aspirated and Krebs-Ringer HEPES buffer (116 mM NaCl,
488 25 mM HEPES, 4 mM KCl, 2 mM D-glucose, 1.8 mM $CaCl_2$, 1 mM $MgCl_2$) supplemented with 1% (w/v)
489 bovine serum albumin (KRHB) was added. This process was repeated three times to remove contaminating
490 stromal vascular cells. To ensure consistent cell seeding, isolated adipocytes were packed via centrifugation
491 for 3 minutes at 100 g and the resulting layers of aqueous buffer and free lipid were aspirated before use as
492 described[21]. All subsequent handling of isolated adipocytes was performed with wide bore pipette tips.

Size sorting of primary adipocytes

495 To separate adipocytes by size, isolated cells were placed in a 125 mL separatory funnel (ThermoFisher
496 #4301-0125) along with 50 mL of KRHB. The funnel was gently inverted several times to resuspend the
497 adipocytes. After 35 seconds, the bottom 35 mL of cell suspension was eluted and passed through a 50 µm
498 cell strainer (pluriSelect #435005003). 35 mL of fresh KRHB was added to the funnel and this process was
499 repeated. Adipocytes that passed through the cell strainers were pooled and used as the "small" fraction for
500 all experiments. 35 mL of fresh KRHB was then added to the funnel before gently inverting several times.
501 After 15 seconds, the bottom 35 mL of cell suspension was eluted and discarded. This process was repeated
502 two additional times to remove cells of intermediate size. The remaining adipocytes were treated as the
503 "large" fraction for all experiments.

Assessment of primary adipocyte viability

506 To assess cell viability after isolation and sorting, unfixed adipocytes were stained with 2 µg/mL Hoechst
507 33342 (ThermoFisher #H3570) and 2 µg/mL propidium iodide (ThermoFisher #P3566) in DMEM/F12 for 30
508 minutes at 37°C protected from light. To image floating adipocytes, an imaging chamber was created by
509 stacking two 120 µm-thick imaging spacers (GraceBio #654004) on top of a microscope slide. Primary
510 adipocytes were diluted in DMEM/F12, added as a 30 µL drop to the center of the spacers, and covered with
511 a glass coverslip for imaging. The percentage of live adipocytes was quantified as the number of cells with
512 propidium iodide-negative nuclei over the number of cells with Hoechst-positive nuclei. The imaging chamber
513 was cleaned with 70% (v/v) ethanol, rinsed with 1x PBS, and dried between samples.

RNA sequencing and analysis

516 For sample collection, 100 µL of packed adipocytes were lysed in 1 mL Qiazol (Qiagen #79306), incubated
517 for 5 minutes at room temperature, and then stored at –80°C until RNA extraction. RNA extraction was
518 performed using an RNeasy Lipid Tissue Mini Kit (Qiagen #74804) according to manufacturer protocols. RNA
519 concentration, 260/280 purity, and 260/230 purity were assessed via a NanoDrop Spectrophotometer
520 (ThermoFisher) and RNA concentration and quality were assessed via a 4200 TapeStation System (Agilent).
521 Libraries were then prepared using a QuantSeq FWD Kit (Lexogen) and sequenced as 86 bp single-end
522 reads on a NextSeq500 System (Illumina). Reads were trimmed using fastp (v.0.23.4) and aligned to the
523 mouse reference genome GRCm39 (GENCODE) using STAR (v.2.7.10b). Reads were counted using the
524 GeneCounts feature of STAR and differential expression analysis was performed with DESeq2 (v.1.40.2).
525 Differentially expressed genes were defined as those with an absolute log_2 fold-change greater than 1 and
526 adjusted p-value less than 0.05. Heat maps were generated using pheatmap (v.1.0.12), volcano plots were
527 generated using EnhancedVolcano (v.1.18.0), and principal component analysis plots were generated using
528 PCAtools (v.2.12.0). Gene set enrichment analysis (GSEA) was performed using fgsea (v.1.26.0) by
529 providing a list of ranked genes from the DESeq2 statistic column.

Collection of mastectomy patient data

532 The Institutional Review Boards of Memorial Sloan Kettering Cancer Center (IRB 10-040) and Weill Cornell
533 Medicine (IRB 1004010984-01) approved the collection of non-tumor breast tissue and blood under a

534 biospecimen acquisition protocol. Informed consent was obtained from all participants. In total, 196 patients
535 underwent mastectomy for breast cancer risk reduction or treatment. Height and weight were recorded prior
536 to surgery and used to calculate body mass index (BMI). Standard definitions were used to categorize BMI
537 as normal weight (BMI < 25), overweight (BMI 25.0–29.9), or obese (BMI ≥ 30). All data were reviewed for
538 accuracy independently by research staff and a physician. On the day of mastectomy, paraffin blocks and
539 snap frozen samples were prepared from breast WAT. If a tumor was present, samples were taken from an
540 uninvolved quadrant of the breast. Two hematoxylin- and eosin-stained sections were generated from
541 formalin-fixed, paraffin-embedded breast tissue in order to measure adipocyte diameters as previously
542 described[46]. The sections were photographed with a 20x objective using an Olympus BX43 or BX50
543 microscope equipped with an Olympus DP27 or MicroFire (Optronics) digital camera, respectively. Mean
544 diameters were calculated using measurements for each patient using the linear dimensional tool in the
545 Canvas 11 Software (ACD Systems International, Inc.), which was calibrated using a microscope stage
546 micrometer.

548 On the day of surgery, a 30 mL fasting blood sample was obtained preoperatively. Centrifugation was used
549 to separate blood into serum and plasma within 3 hours of collection and stored at −80°C. Serum levels of
550 triglycerides and high-density lipoprotein (HDL) cholesterol were determined in the Memorial Sloan Kettering
551 Cancer Center Clinical Chemistry Lab.

553 Human RNA sequencing data have been previously published[22] and were deposited to the European
554 Genome-Phenome Archive (EGA) under accession number EGAS00001004665.

556 ### Preparation of elastomer microwells
557 Elastomer microwells for *ex vivo* culture of primary adipocytes were prepared as previously described[21].
558 Briefly, SYLGARD 184 silicone elastomer (Ellsworth Adhesives #4019862) was cast in 1.5 mm-thick slabs
559 according to manufacturer protocols. 10 mm outer diameter, 6 mm inner diameter elastomer rings were cut
560 and bonded to glass coverslips using a plasma cleaner (Harrick Plasma). The rings were treated with 1%
561 (v/v) poly(ethylenimine) (Sigma-Aldrich #181978), 0.1% (v/v) glutaraldehyde (ThermoFisher
562 #ICN19859580), and washed three times with sterile water to facilitate covalent adhesion of adipocyte-
563 collagen gels.

565 ### Preparation of adipocyte-collagen gels
566 For *ex vivo* culture, packed adipocytes were mixed into a collagen gel at a 3:1 ratio (v/v) using wide-bore
567 pipette tips as previously described[21]. Briefly, to prepare the collagen gel, collagen type I (VWR #47747-218)
568 was diluted to a final concentration of 2.5 mg/mL in DMEM/F12. This solution was kept on ice and neutralized
569 with 1N NaOH to begin polymerization immediately before the addition of packed adipocytes. During
570 polymerization, the adipocyte-collagen gels were inverted every 2 minutes for 20 minutes at room
571 temperature to ensure an even distribution of cells. The resulting gels were submerged in DMEM/F12 and
572 cultured for up to 5 days at 37°C.

574 ### Coculture studies
575 For coculture studies, 30,000 breast cancer cells (MDA-MB-231, MCF7, PY8119, or EO771) were plated per
576 well in a 24-well plate containing 12 mm glass coverslips (Chemglass #CLS-1760-012) coated with 30 µg/mL
577 collagen type I (VWR #47747-218). The following day, primary adipocytes were isolated and adipocyte-
578 collagen gels in elastomer microwells were prepared. One cancer cell coverslip and one adipocyte-collagen
579 gel were placed into each well of a 12-well plate along with 1.5 mL of DMEM/F12. Cancer cells and primary
580 adipocytes were cocultured together for 72 hours. Cancer cells were then reserved for functional studies or
581 fixed in 4% (w/v) paraformaldehyde for imaging.
582

EdU proliferation assays

For proliferation studies, precultured cancer cells were trypsinized and reseeded at 30,000 cells per well in a 24-well plate containing 12 mm glass coverslips coated with 30 µg/mL collagen type I (VWR #47747-218). Once adherent, replated tumor cells were incubated in low-serum DMEM/F12 for 12 hours. The following morning, proliferating tumor cells were labeled with the Alexa Fluor 647 EdU Kit (ThermoFisher #C10340) according to manufacturer protocols. Briefly, a 20 µM EdU solution was prepared in low-serum DMEM/F12 and added 1:1 to existing media to achieve a final concentration of 10 µM EdU. Cancer cells were incubated for 2 hours at 37°C before proceeding with fixation, permeabilization, and detection of incorporated EdU. Cancer cells were co-stained with Hoechst 33342 (ThermoFisher #H3570) and BODIPY 493/503 (ThermoFisher #D3922). For inhibitor studies, 40 µM etomoxir (Millipore #236020) or DMSO vehicle were added with the low-serum DMEM/F12 after precultured cancer cells adhered to collagen-coated glass coverslips.

Tissue-culture insert migration assays

For migration assays, precultured cancer cell coverslips were transferred to a 24-well plate and incubated in low-serum DMEM/F12 for 12 hours. The following morning, 8 µm pore tissue-culture inserts (VWR #29442-120) were coated with 30 µg/mL collagen type I (VWR #47747-218) and placed in 24-well plates containing 600 µL of DMEM/F12. Precultured cancer cells were then trypsinized and reseeded at 30,000 cells per tissue-culture insert in 100 µL of low-serum DMEM/F12 to establish a serum gradient. Cancer cells were allowed to migrate for 12 hours at 37°C. Cells were then fixed with 4% paraformaldehyde and a cotton swab was used to gently remove cells from the upper side of the insert membrane. The underside of each membrane was stained with DAPI (ThermoFisher #D1306) and imaged to quantify the number of transmigrated cancer cells. For inhibitor studies, 40 µM etomoxir (Millipore #236020) or DMSO vehicle were added to the low-serum DMEM/F12 when reseeding precultured cancer cells into tissue-culture inserts.

Mitochondrial imaging in live breast cancer cells

To assess co-localization of breast cancer cell lipid droplets and mitochondria after coculture with adipocytes, precultured MDA-MB-231s were reseeded at 100,000 cells per glass-bottom petri dish (World Precision Instruments #FD35-100) coated with 30 µg/mL collagen type I (VWR #47747-218). Precultured cancer cells were then stained with 200 nM MitoView 640 (Biotium #70082) for 12 hours. Live samples were co-stained with 2 µg/mL Hoechst 33342 and 2.5 µg/mL BODIPY 493/503 for 30 minutes, washed twice with DMEM/F12, and imaged on an inverted Zeiss LSM 880 confocal microscope with an incubation chamber.

Pre-labeling lipid to monitor transfer from adipocytes to breast cancer cells

For pre-labeling experiments, primary adipocytes were stained in suspension with 2.5 µg/mL BODIPY 493/503 for 30 minutes and washed three times with KRHB prior to embedding into collagen gels. Pre-labeled adipocytes were then cocultured with MDA-MB-231 breast cancer cells as described. After 48 hours, breast cancer cells were fixed with 4% (w/v) paraformaldehyde in 1x PBS and counterstained with 2.5 µg/mL DAPI and 165 µM Alexa Fluor 568 phalloidin. Breast cancer cells were then imaged on an inverted Zeiss LSM 880 confocal microscope to detect the presence of BODIPY-labeled neutral lipid.

Sample fixation, permeabilization, and fluorescence staining

Samples were fixed in cold 4% (w/v) paraformaldehyde (Electron Microscopy Sciences #19208) in 1x PBS for 15 minutes at room temperature. Samples were washed twice with 1x PBS and permeabilized with 0.1% Triton X-100 (v/v) (ThermoFisher #A16046-AE) in 1x PBS supplemented with 1% (w/v) bovine serum albumin (BSA) (ThermoFisher #BP1600-100) for 15 minutes at room temperature. Samples were washed twice with 1x PBS and then stained with one or more of the indicated dyes as follows: 0.165 µM Alexa Fluor 488 phalloidin (ThermoFisher #A12379) or 0.165 µM Alexa Fluor 568 phalloidin (ThermoFisher #A12380) in 1x PBS with 1% BSA for 1 hour at room temperature; 2.5 µg/mL 4,4-difluoro-1,3,5,7,8-pentamethyl-4-bora-

632 3a,4a-diaza-*s*-indacene (BODIPY 493/503) in 1x PBS with 1% BSA for 30 minutes at room temperature; 2.5
633 µg/mL 4',6-diamidino-2-phenylindole, dihydrochloride (DAPI) (ThermoFisher #D1306) in 1x PBS with 1%
634 BSA for 30 minutes at room temperature. Samples were then washed twice with 1x PBS and stored in 1x
635 PBS at 4°C until imaged.
636
637 ### Confocal microscopy and image analysis
638 Images were acquired on an inverted or upright Zeiss LSM 880 confocal microscope using either a 10x/0.45
639 W C-Apochromat objective, 20x/0.5 EC Plan-Neofluar objective, 20x/1.0 W Plan-Apochromat objective,
640 40x/1.2 W C-Apochromat objective, or 63x/1.4 O Plan-Apochromat objective. All images analysis was
641 performed in QuPath[47] and ImageJ (National Institutes of Health). For semi-automated quantification of
642 adipocytes, cancer cell lipid droplets, and 3T3-L1 lipid droplets, the AdipoQ ImageJ plug-in[48] was used.
643 Manuscript figures were prepared using Adobe Photoshop, Adobe Illustrator, and Biorender.com.
644
645 ### Substrate oxidation stress test
646 To assess ATP production and FAO, cancer cell metabolism was probed using a Seahorse XFe 96
647 Extracellular Flux Analyzer (Agilent) and Seahorse XF Long Chain Fatty Acid Oxidation Stress Test Kit
648 (Agilent #103672-100). Control or precultured cancer cells were seeded at 20,000 cells per well in an XFe96
649 Cell Culture Microplate (Agilent #103794-100) in DMEM/F12 and allowed to adhere overnight. The following
650 morning, media was changed to Seahorse XF DMEM, pH 7.4 (Agilent #103680-100), and manufacturer
651 protocols were followed to complete the Long Chain Fatty Acid Oxidation Stress Test Kit. Inhibitor
652 concentrations of 4 µM for etomoxir, 1.5 µM for oligomycin, 1 µM for FCCP, and 0.5 µM for rotenone/antimycin
653 A were used. After the stress test was complete, DNA was extracted using lysis buffer (25 mM Tris-HCl, 0.4
654 M NaCl, 0.5% (w/v) sodium dodecyl sulfate) and total DNA content per well was measured using the
655 QuantiFluor dsDNA Assay (VWR #PAE2671) for data normalization.
656
657 ### Glycerol assay
658 Conditioned media from cancer cell and adipocyte-collagen gel cocultures was collected after 72 hours and
659 stored at –20°C until processed. Once thawed, the relative degree of lipolysis during culture was estimated
660 by measuring the concentration of glycerol in the conditioned media using the Adipolysis Assay Kit (Sigma-
661 Aldrich #MAK313) according to manufacturer protocols.
662
663 ### Isolation of extracellular vesicles from adipocyte-conditioned media
664 Adipocyte-collagen gels were cultured in 24-well plates containing 750 µL of exosome-depleted DMEM/F12
665 to generate conditioned media. Extracellular vesicles were then isolated from conditioned media using
666 modified versions of published protocols[49]. Briefly, conditioned media was centrifugated at 300 x g at 4°C for
667 10 minutes to remove dead cells and other debris. The resulting supernatant was transferred to a new tube
668 and centrifuged at 3000 x g at 4°C for 30 minutes to remove apoptotic bodies. The resulting supernatant was
669 transferred to a new tube and combined at a 1:1 ratio (v/v) with 16% (w/v) PEG 6000 (Sigma-Aldrich #82160)
670 in 1 M NaCl for a final concentration of 8% PEG 6000 in 0.5 M NaCl. The resulting solution was inverted
671 several times and incubated at 4°C for at least 12 hours to precipitate soluble factors and extracellular
672 vesicles. The precipitate was then pelleted via centrifugation at 3220 x g at 4°C for 1 hour. After aspirating
673 the supernatant containing PEG 6000, the pellet was resuspended in 2 mL of filtered 1x PBS and
674 ultracentrifuged in a TLS-55 swinging-bucket rotor (Beckman Coulter #346936) at 100,000 x g at 4°C for 4
675 hours. The supernatant containing soluble factors was discarded and the extracellular vesicle pellet was
676 resuspended in 1 mL of filtered 1x PBS for nanoparticle tracking analysis.
677
678 ### Nanoparticle tracking analysis of extracellular vesicles
679 Isolated extracellular vesicles were quantified via nanoparticle tracking analysis (NTA) using a Malvern
680 NanoSight NS300. Samples were passed through the NanoSight flow cell using the included syringe pump

681 at a flow rate of 50. At least 10 videos, each 30 seconds in length, were acquired with a 488 nm laser per
682 sample. The concentration and size distribution of vesicles in each sample were then calculated using the
683 Malvern Nanoparticle Tracking Analysis Software.

684

685 ### *Western blotting of vesicle markers*
686 Sorted adipocytes for each condition, as well as preparations of the extracellular vesicles these cells
687 generated, were lysed using lysis buffer (25 mM Tris, 100 mM NaCl, 1% Triton X-100, 1 mM EDTA, 1.0 µg/
688 mL each of aprotinin and leupeptin, 1.0 mM β-glycerol phosphate, and 1.0 mM DTT). Protein concentrations
689 of the cell (whole cell lysates; WCLs) and extracellular vesicle lysates were determined using the Bio-Rad
690 Protein Assay Dye (Bio-Rad) and a spectrophotometer at a wavelength of 595. The lysates were normalized
691 based on protein concentration and resolved on 4-20% SDS-PAGE gels (Invitrogen). The gels were
692 transferred to PVDF membranes (Thermo-Fisher Scientific), and the membranes were blocked in 5.0%
693 bovine serum albumin (BSA) in TBST buffer (20 mM Tris, 135 mM NaCl, and 0.02% Tween) for 1 hour at
694 room temperature. The membranes were then incubated with one of the following primary antibodies diluted
695 in TBST overnight at 4°C: FAK antibody (1:1000 dilution; Cell Signaling Technologies, #3285) and FLOT2
696 antibody (1:1000 dilution; Cell Signaling Technologies, #3436). The next day, the membranes were washed
697 3 times for 5 minutes with TBST before being incubated with HPR-conjugated secondary antibodies diluted
698 in TBST for 1 hour at room temperature. The membranes were again washed with TBST 3 times for 5
699 minutes and exposed to ECL reagents (Bio-Rad). Images of the membranes were obtained using X-ray film
700 (The Lab Depot).

701

702 ### *Breast cancer cell treatment with adipocyte-derived vesicles*
703 For studies requiring treatment with adipocyte-derived extracellular vesicles, conditioned media was
704 processed as described for analysis of vesicles through PEG 6000 precipitation and centrifugation at 3220 x
705 g. The precipitate was then resuspended in 2 mL of exosome-depleted DMEM/F12 instead of 1x PBS. This
706 solution was ultracentrifuged in a TLS-55 swinging-bucket rotor (Beckman Coulter) at 100,000 x g at 4°C for
707 4 hours. The resulting extracellular vesicle pellet was resuspended in 2 mL of exosome-depleted DMEM/F12
708 for downstream use.

709

710 ### *Extracellular vesicle treatment and DGAT1/2 inhibitor studies*
711 For studies of lipid uptake from adipocyte-derived extracellular vesicles, 30,000 MDA-MB-231 breast cancer
712 cells were plated per well in a 24-well plate containing 12 mm glass coverslips coated with 30 µg/mL collagen
713 type I (VWR #47747-218). The following day, vesicles were applied to the cancer cells with 40 µM iDGAT1
714 (PF 04620110) (Tocris #1109276-89-2) and 40 µM iDGAT2 (PF 06424439) (Tocris #1469284-79-4) or an
715 equivalent volume of DMSO vehicle. Treatment was applied such that each glass coverslip seeded with
716 breast cancer cells received vesicles collected from one adipocyte-collagen gel over 24 hours. Breast cancer
717 cells were incubated with vesicles for 24 hours at 37°C and then fixed with 4% (w/v) paraformaldehyde in 1x
718 PBS for analysis of lipid uptake via fluorescence microscopy.

719

720 ### *Lipid extraction and derivatization for lipidomics*
721 100 µL of flash-frozen adipocytes were lysed in 1 mL 66% methanol (v/v) in 0.1 M potassium phosphate
722 buffer (pH 6.8) by vortexing twice on high for 20 seconds each. A 10 µL aliquot from each lysate was reserved
723 for total protein quantification using BCA assay (Thermo Fisher, #23225). The remaining lysate was
724 transferred to 13 x 100 mm borosilicate glass tubes (Fisher Scientific, #14-961-27), acidified with 10 µL of
725 1N HCl, and briefly vortexed. Total lipids were extracted twice with 1 mL of isooctane:ethyl acetate (3:1 v/v)
726 and once with 1 mL hexanes. Each extraction was followed by 10-15 seconds of vortexing and then
727 centrifugation at 2000 x g for 1 minute to ensure phase separation. The upper organic phases from all
728 extractions were combined in fresh 13 x 100 mm borosilicate glass tubes, evaporated under gaseous
729 nitrogen, and resuspended in 300 µL isooctane. For the non-esterified fatty acid (NEFA) fraction, 100 µL of

730 the total lipid extract was transferred to a new glass tube, 25 ng internal stable isotope standard was added,
731 evaporated under nitrogen, and resuspended in 25 μL of 1% pentafluorobenzyl bromide in acetonitrile (v/v).
732 An equal volume of 1% diisopropylethylamine in acetonitrile (v/v) was added, followed by a 30-minute
733 incubation at 25°C. The resulting pentafluorobenzyl-fatty acid derivatives were dried under nitrogen,
734 resuspended in 100 μL of hexanes, and prepared for injection into the GC-MS. For the total fatty acid (TFA)
735 fraction, 10 μL of the total lipid extract was transferred to a Teflon-lined glass tube, mixed with 75 ng of the
736 stable isotope internal standard, and dried under nitrogen. Samples were resuspended in 500 μL of ethanol,
737 and 500 μL of 1 M NaOH was added to saponify over 30 minutes at 90°C. After cooling, samples were
738 acidified with 550 μL of 1 M HCl and extracted twice with 1.5 mL of hexanes. The extracts were dried under
739 nitrogen and derivatized as described above. TFA samples were resuspended in 300 μL of hexanes for GC-
740 MS injection.
741

742 ***GC-MS conditions and data acquisition***
743 For both the NEFA and TFA fractions, 1 μL of the pentafluorobenzyl-fatty acid derivatives was injected into
744 an Agilent 8890 GC system coupled to a 5977B MS detector, using a DB-1MS UI column (Agilent, #122-
745 0112UI). The GC temperature program consisted of an initial hold at 80°C for 3 minutes, followed by a ramp
746 of 30°C per min to 125°C, and a second ramp of 25°C per min to 320°C with a final hold of 2 minutes.
747 Methane was the carrier gas, flowing at 1.5 mL per min. Data were acquired in full-scan negative chemical
748 ionization mode, using m/z for acyl chain lengths ranging from 8 to 22 carbons and unsaturation. Peak areas
749 of analytes and internal standards were measured, and the ratio of analyte-derived ion areas to internal
750 standard areas was calculated for quantification relative to each standard curve[50,51].
751

752 ***Statistical analysis***
753 All experiments were performed with at least three biological replicates unless otherwise noted. Data with
754 two conditions were evaluated with a nonparametric Mann-Whitney U test unless otherwise noted. Data with
755 three or more conditions were evaluated with either a standard or nested one-way ANOVA with Tukey multiple
756 comparisons test unless otherwise noted. P-values less than 0.05 were considered statistically significant.
757 Unless otherwise noted, all data are plotted as means with standard deviations. All statistical analysis was
758 performed using GraphPad Prism (v.10.2.3) or R (v.4.3.1).

759 **References**

760 1. Products - Data Briefs - Number 508 - September 2024.

761   https://www.cdc.gov/nchs/products/databriefs/db508.htm (2024) doi:10.15620/cdc/159281.

762 2. Obesity and Cancer Fact Sheet - NCI. https://www.cancer.gov/about-cancer/causes-

763   prevention/risk/obesity/obesity-fact-sheet (2022).

764 3. González-Muniesa, P. *et al*. Obesity. *Nature Reviews Disease Primers* **3**, 1–18 (2017).

765 4. Fuentes-Mattei, E. *et al*. Effects of Obesity on Transcriptomic Changes and Cancer Hallmarks in

766   Estrogen Receptor–Positive Breast Cancer. *JNCI: Journal of the National Cancer Institute* **106**,

767   dju158 (2014).

768 5. Wang, T. *et al*. JAK/STAT3-Regulated Fatty Acid β-Oxidation Is Critical for Breast Cancer Stem Cell

769   Self-Renewal and Chemoresistance. *Cell Metab* **27**, 136-150.e5 (2018).

770 6. Piening, A. *et al*. Obesity-related T cell dysfunction impairs immunosurveillance and increases

771   cancer risk. *Nat Commun* **15**, 2835 (2024).

772 7. Shook, B. A. *et al*. Dermal Adipocyte Lipolysis and Myofibroblast Conversion Are Required for

773   Efficient Skin Repair. *Cell Stem Cell* **26**, 880-895.e6 (2020).

774 8. Zhu, Q. *et al*. Adipocyte mesenchymal transition contributes to mammary tumor progression. *Cell*

775   *Reports* **40**, 111362 (2022).

776 9. Emont, M. P. *et al*. A single-cell atlas of human and mouse white adipose tissue. *Nature* **603**, 926–

777   933 (2022).

778 10.   Bäckdahl, J. *et al*. Spatial mapping reveals human adipocyte subpopulations with distinct

779   sensitivities to insulin. *Cell Metabolism* (2021) doi:10.1016/j.cmet.2021.07.018.

780 11.   Almekinders, M. M. M. *et al*. Breast adipocyte size associates with ipsilateral invasive breast

781   cancer risk after ductal carcinoma in situ. *npj Breast Cancer* **7**, 1–10 (2021).

782 12.   Ghaben, A. L. & Scherer, P. E. Adipogenesis and metabolic health. *Nat. Rev. Mol. Cell Biol.* **20**,

783   242–258 (2019).

784   13.   Acosta, J. R. *et al.* Increased fat cell size: a major phenotype of subcutaneous white adipose

785   tissue in non-obese individuals with type 2 diabetes. *Diabetologia* **59**, 560–570 (2016).

786   14.   Iyengar, N. M. *et al.* Metabolic Obesity, Adipose Inflammation and Elevated Breast Aromatase

787   in Women with Normal Body Mass Index. *Cancer Prevention Research* **10**, 235–243 (2017).

788   15.   Harms, M. J. *et al.* Mature Human White Adipocytes Cultured under Membranes Maintain

789   Identity, Function, and Can Transdifferentiate into Brown-like Adipocytes. *Cell Rep* **27**, 213-225.e5

790   (2019).

791   16.   Dufau, J. *et al.* In vitro and ex vivo models of adipocytes. *American Journal of Physiology-Cell*

792   *Physiology* **320**, C822–C841 (2021).

793   17.   Dirat, B. *et al.* Cancer-associated adipocytes exhibit an activated phenotype and contribute to

794   breast cancer invasion. *Cancer Res.* **71**, 2455–2465 (2011).

795   18.   Liu, S. *et al.* Breast adipose tissue-derived extracellular vesicles from obese women alter

796   tumor cell metabolism. *EMBO reports* **24**, e57339 (2023).

797   19.   Balaban, S. *et al.* Adipocyte lipolysis links obesity to breast cancer growth: adipocyte-derived

798   fatty acids drive breast cancer cell proliferation and migration. *Cancer Metab* **5**, 1 (2017).

799   20.   Park, J., Morley, T. S., Kim, M., Clegg, D. J. & Scherer, P. E. Obesity and cancer—mechanisms

800   underlying tumour progression and recurrence. *Nature Reviews Endocrinology* **10**, 455–465 (2014).

801   21.   Beeghly, G. F., Deng, J. & Fischbach, C. Protocol to fabricate elastomer microwells for three-

802   dimensional culture of primary adipocytes. *STAR Protoc* **5**, 103264 (2024).

803   22.   Cho, B. A. *et al.* Blood biomarkers reflect the effects of obesity and inflammation on the

804   human breast transcriptome. *Carcinogenesis* **42**, 1281–1292 (2021).

805   23.   Zhang, Y. *et al.* Positional cloning of the mouse obese gene and its human homologue. *Nature*

806   **372**, 425–432 (1994).

807   24.   Velickovic, K. *et al.* Leptin deficiency impairs adipogenesis and browning response in mouse

808   mesenchymal progenitors. *European Journal of Cell Biology* **102**, 151342 (2023).

809   25.   Jernås, M. *et al.* Separation of human adipocytes by size: hypertrophic fat cells display distinct

810   gene expression. *FASEB J* **20**, 1540–1542 (2006).

811   26.   Hara, Y. *et al.* Rho and Rho-kinase activity in adipocytes contributes to a vicious cycle in

812   obesity that may involve mechanical stretch. *Sci Signal* **4**, ra3 (2011).

813   27.   Hansson, B. *et al.* Adipose cell size changes are associated with a drastic actin remodeling. *Sci*

814   *Rep* **9**, 12941 (2019).

815   28.   Wang, S. *et al.* Adipocyte Piezo1 mediates obesogenic adipogenesis through the FGF1/FGFR1

816   signaling pathway in mice. *Nat Commun* **11**, 2303 (2020).

817   29.   Aboy-Pardal, M. C. M. *et al.* Plasma membrane remodeling determines adipocyte expansion

818   and mechanical adaptability. *Nat Commun* **15**, 10102 (2024).

819   30.   Xia, W. *et al.* Obesity causes mitochondrial fragmentation and dysfunction in white adipocytes

820   due to RalA activation. *Nat Metab* **6**, 273–289 (2024).

821   31.   Baldini, F. *et al.* Adipocyte hypertrophy parallels alterations of mitochondrial status in a cell

822   model for adipose tissue dysfunction in obesity. *Life Sciences* **265**, 118812 (2021).

823   32.   Ling, L. *et al.* Obesity-Associated Adipose Stromal Cells Promote Breast Cancer Invasion

824   through Direct Cell Contact and ECM Remodeling. *Advanced Functional Materials* **n/a**, 1910650

825   (2020).

826   33.   Seo, B. R. *et al.* Collagen microarchitecture mechanically controls myofibroblast

827   differentiation. *PNAS* (2020) doi:10.1073/pnas.1919394117.

828   34.   Loo, S. Y. *et al.* Fatty acid oxidation is a druggable gateway regulating cellular plasticity for

829   driving metastasis in breast cancer. *Science Advances* **7**, eabh2443 (2021).

830   35.   Lazar, I. *et al.* Adipocyte Exosomes Promote Melanoma Aggressiveness through Fatty Acid

831   Oxidation: A Novel Mechanism Linking Obesity and Cancer. *Cancer Res* **76**, 4051–4057 (2016).

832   36.   Zhang, M. *et al.* Adipocyte-Derived Lipids Mediate Melanoma Progression via FATP Proteins.

833   *Cancer Discov* **8**, 1006–1025 (2018).

834   37.   Flaherty, S. E. *et al*. A lipase-independent pathway of lipid release and immune modulation by

835   adipocytes. *Science* **363**, 989–993 (2019).

836   38.   Wang, Y. Y. *et al*. Mammary adipocytes stimulate breast cancer invasion through metabolic

837   remodeling of tumor cells. *JCI Insight* **2**, e87489 (2017).

838   39.   Sezgin, E., Levental, I., Mayor, S. & Eggeling, C. The mystery of membrane organization:

839   composition, regulation and roles of lipid rafts. *Nat Rev Mol Cell Biol* **18**, 361–374 (2017).

840   40.   Yoon, H., Shaw, J. L., Haigis, M. C. & Greka, A. Lipid metabolism in sickness and in health:

841   Emerging regulators of lipotoxicity. *Mol Cell* **81**, 3708–3730 (2021).

842   41.   Rudalska, R. *et al*. LXRα activation and Raf inhibition trigger lethal lipotoxicity in liver cancer.

843   *Nat Cancer* **2**, 201–217 (2021).

844   42.   Tan, Y. *et al*. Metabolic reprogramming from glycolysis to fatty acid uptake and beta-oxidation

845   in platinum-resistant cancer cells. *Nat Commun* **13**, 4554 (2022).

846   43.   Poggio, F. *et al*. Platinum-based neoadjuvant chemotherapy in triple-negative breast cancer: a

847   systematic review and meta-analysis. *Annals of Oncology* **29**, 1497–1508 (2018).

848   44.   Galarraga, M. *et al*. Adiposoft: automated software for the analysis of white adipose tissue

849   cellularity in histological sections. *J Lipid Res* **53**, 2791–2796 (2012).

850   45.   Sieckmann, K. *et al*. AdipoQ—a simple, open-source software to quantify adipocyte

851   morphology and function in tissues and in vitro. *Mol Biol Cell* **33**, br22 (2022).

852   46.   Iyengar, N. M. *et al*. Menopause is a determinant of breast adipose inflammation. *Cancer Prev

853   Res (Phila)* **8**, 349–358 (2015).

854   47.   Bankhead, P. *et al*. QuPath: Open source software for digital pathology image analysis. *Sci Rep*

855   **7**, 16878 (2017).

856   48.   Sieckmann, K. *et al*. AdipoQ—a simple, open-source software to quantify adipocyte

857   morphology and function in tissues and in vitro. *MBoC* **33**, br22 (2022).

858   49.   Rider, M. A., Hurwitz, S. N. & Meckes, D. G. ExtraPEG: A Polyethylene Glycol-Based Method for

859   Enrichment of Extracellular Vesicles. *Sci Rep* **6**, 23978 (2016).

860   50.   Rudolph, M. C. *et al*. Mammalian Fatty Acid Synthase Activity From Crude Tissue Lysates

861   Tracing [13C]-Substrates Using GC Mass Spectrometry. *Anal Biochem* **428**, 158–166 (2012).

862   51.   Varshney, R. *et al*. Neonatal intake of Omega-3 fatty acids enhances lipid oxidation in

863   adipocyte precursors. *iScience* **26**, 105750 (2023).